A Model-Based System Engineering Approach for the Virtual Prototyping of an Electric Vehicle of Class L7

Carmine Maria Pappalardo, Nicola Lombardi, Domenico Guida

Abstract—**This study is aimed at creating an accurate mathematical model concerning an electric vehicle of class L7. This category includes quadricycles having a mass less than 400 kg, batteries excluded, and power below 15 kW. To this end, an electromechanical model with three degrees of freedom is developed in the Matlab-Simulink virtual environment employing the Simscape library. In the mechanical model developed in this investigation, the main degrees of freedom considered are the forward advancement, the vertical displacement, and the angular pitch. Furthermore, two additional degrees of freedom are also included in the dynamical model in order to take into account the suspension displacements as well as the dynamic effects induced by the stiffness and damping characteristics of the tires. The behavior of the contact force generated by the interaction of the tires with the road profile is described by using the Pacejka Magic Formula. On the other hand, the propulsion unit is modeled considering three different configurations: the first scheme is composed of a central electric engine having a fixed gearbox and a mechanical differential; the second design solution is similar to the previous one but is equipped with a two-speed gearbox; finally, the third configuration consists of two separate electric engines. In all the design configurations mentioned before, the vehicle can be controlled by providing the driver inputs, by controlling the cruising speed, or by ensuring that the vehicle follows a specific driving cycle. By means of a comparative analysis performed between the three different design configurations, the proposed virtual model allows for identifying which design solution is the most appropriate, thereby reducing the time required in the design phases and also simplifying the entire process development. In conclusion, it can be stated that the virtual prototype developed in this work is able to satisfactorily predict the dynamical behavior and the energy consumption of the L7 class vehicle of interest.**

Index Terms—**Model-Based System Engineering, Virtual Prototyping, Engineering Mechanics, Electric Systems, L7 Class Light Vehicles, MATLAB-Simulink Modeling.**

I. Introduction

The present paper deals with the virtual design and the computer development of a dynamical model of an electric vehicle of category L7 by using a model-based system engineering approach. This introductory section provides background information, the identification of the challenges encountered in addressing the problem at hand, a short literature review on research works that are relevant for this study, the scope and contributions of this investigation, and the organization of the manuscript.

C. M. Pappalardo is with the *Department of Industrial Engineering, University of Salerno*, Via Giovanni Paolo II, 132, 84084 Fisciano, Salerno, ITALY (corresponding author, email: cpappalardo@unisa.it).

N. Lombardi is with the *Spin-Off MEID4 s.r.l., University of Salerno*, Via Giovanni Paolo II, 132, 84084 Fisciano, Salerno, ITALY (email: n.lombardi7@studenti.unisa.it).

D. Guida is with with the *Department of Industrial Engineering, University of Salerno*, Via Giovanni Paolo II, 132, 84084 Fisciano, Salerno, ITALY (email: guida@unisa.it).

A. Reference Context and Research Significance

In the modern mechanical engineering industry, products are becoming more demanding and sophisticated at an exponential rate. The design and development of these systems are also becoming more challenging because of the stringent requirements on performance, security, and reliability aspects. Furthermore, the complete cycles of product development are reducing their duration since it is necessary to construct more complex systems with fewer defects and in less time. A possible solution for addressing these difficult problems is to adopt a model-based system engineering approach which proved to be effective especially in the complex process of the automobile design [1], [2]. The system engineering method can be considered as the multidisciplinary approach capable of converting a set of functional needs into a coherent and systematic solution aimed at addressing those requirements [3]–[5]. Among the others, this process involves several different activities such as to determine the main goals which must be supported by a given system, state the system requirements, devise alternative designs, assess the performance of the viable alternatives, allocate resources to the mechanical components, integrate the individual parts separately constructed into the assembled system, verify that the system functional requirements are effectively met, and include in the whole loop the control procedures needed to handle in synergy the overall technical efforts [6]–[11]. The model-based system engineering approach makes use of computer models of the mechanical systems of interest for addressing technologically challenging problems in conjunction with virtual prototyping techniques, which are both of interest for the object of this investigation.

In the last thirty years, the virtual prototyping of mechanical systems based on dynamical simulations has become ubiquitous in all the industrial fields related to mechanical engineering. By performing numerical experiments based on virtual models, the mechanical engineer is able to gain insights into the fundamental properties of the system of interest for a particular application in several realistic scenarios. By doing so, alternative concepts for the design solution of interest can be tested using simple mathematical models leading to inexpensive estimations of the required dynamic behavior [12]–[14]. Moreover, once that a virtual model of a real system has been verified experimentally, the validated dynamic analysis is useful for monitoring, diagnostics, and failure prediction of the actual prototypes.

Thus, it is clear that the engineering design process based on computer simulations can be significantly enhanced by the virtual prototyping approach and, therefore, the performance of the final design can be substantially improved by adopting a model-based systematic approach [15]–[17]. Important examples are represented by the use of computer simulations based on the analytical approach developed for multibody mechanical systems, which are thoroughly employed for the dynamic analysis of structural elements, vehicles, robots, and aerospace applications [18]–[22].

As discussed in the excellent essays by Ratti et al. [23], [24], today, modern cities occupy only 2% of the planet surface, they host more than the 50% of the population, their facilities are responsible for the 75% of the total energy consumption, and produce 80% of carbon dioxide. The current situation is, therefore, not sustainable in the long run. The modern design of new cities must follow a more sustainable logic. This issue is interrelated with the mobility problem and the rights of citizens of accessing to efficient means of transportation. In this context, cars, as they are conceived today, represents highly inefficient means of transportation because they are used only for the 5% of their time, on average by one or two people, thereby moving tons of weight for a single individual, while in the remaining 95% of time they stay inactive and occupy, among other things, precious space in the cities. The research work developed in this investigation is collocated in this background context and is focused on one of the viable strategies for contributing to the solution of the important issues mentioned before.

B. Problem Statement

Currently, one of the technologies with the greatest potential in the field of sustainability is electric propulsion. Electric Vehicles (EV) do not emit polluting substances. However, the energy that feeds them globally generates different emissions based on the way in which the same amount of energy is produced. If this energy is obtained through the use of fossil fuels, the result is simply to transfer the emissions from the city to the production plant. On the other hand, if the energy required to power electric vehicles is produced using any renewable form of energy generation, a significant impact on the sustainability of the means of transportation can be achieved. It is, therefore, necessary to globally enhance the synergy between EV and renewable energy production. If these systems were used globally, there would be ideally zero emissions [25], [26].

Another issue to consider is the actual functionality of the vehicles used as means of transportation. As previously stated, regular cars are mostly used for moving an average of one or two individuals. In order to address this problem, different smart solutions can be adopted. For example, among these, the idea of car-sharing is very widespread and welcome from the urban population. This phenomenon consists in the use of a small vehicle shared between a large number of people, which can be comfortably booked through an app from a smartphone. Another viable solution, which is investigated in this paper, is the paradigm shift towards EV. Nevertheless, the adoption and penetration of the EV market are still slowed down by a number of factors. From the economic one, since it is necessary to have an adequate smart grid, large investments are needed on the charging infrastructure, and subsequently the large-scale deployment of these vehicles would entail a significant increase in the power required of the electricity grid, for which, in this way, the planning of a new national energy program becomes necessary. Furthermore, an additional problem which limits the spread of this type of vehicle is an important issue related to the batteries which power the EVs. From the environmental point of view, the extraction of the raw material used for manufacturing several types of batteries and its disposal have a detrimental impact. Moreover, this issue also concerns the cost and functionality of the batteries. Unlike traditional internal combustion vehicles, electric batteries do not guarantee EVs an optimal range of operability due to their low energy density and their relatively slow recharge time. The drawbacks currently associated with EVs represent a strong motivation for a massive increase of the academic and industrial research devoted to this field [27], [28].

If, on the one hand, some issues are at risk of affecting the spread of EVs, on the other hand, there are numerous advantages offered by electric transportation in general. First of all, in addition to not generating emissions locally, electric motors allow for performing the regenerative braking, which consists of energy recovery during vehicle decelerations. This benefit, in particular, is considerable in the cities, where traffic forces continuous small accelerations and braking. Another convenient aspect of EVs is their maintenance, which is cheaper for several reasons. Firstly, the motor and brakes of these vehicles are subject to less wear, and, secondly, some components, such as the starter motor, spark plugs, clutch, radiator, and muffler, are not present in electric cars for which they must not be repaired or replaced. In addition, electric motors, since they are endowed with a large torque at start-up, a high maximum angular velocity, and good efficiency for wide speed ranges, they can be designed according to special configurations without speed change. Therefore, to promote the spread of electric vehicles, several design solutions can be adopted aimed at enhancing the key factors which consist in reducing the weight and cost of the batteries, favoring an increase in the range of the cars, making the EV design lighter, optimizing transmission losses, and improving the regenerative braking system. This paper tries to contribute to these research directions by developing a virtual prototype of an EV of category L7 considering different design solutions analyzed by adopting a system engineering approach [29]–[31].

C. Literature Survey

The multibody approach to vehicle dynamics represents a viable solution procedure for modeling and simulating complex systems in several engineering scenarios. Multibody system dynamics is a transversal field of research concerned with the analysis and the synthesis of the motion of dynamical systems constrained by mechanical joints [32]–[35]. From a wide perspective, multibody systems are mechanical systems having the peculiar feature of being constituted of basic items such as rigid bodies, flexible bodies, kinematic joints, force fields, force elements, control actuators, and motion sensors [36]–[39]. Numerous examples of machines, mechanisms, vehicles, and robots modeled as multibody

systems are present in the literature [40]–[42]. In multibody system dynamics, the most fundamental aspect is the fact that the time evolution of a multibody mechanical system is described by Differential-Algebraic Equations (DAEs) relative to the system motion. The multibody equations of motion are capable of mathematically representing the nonlinear dynamic nature of this class of complex systems. Another important feature that influences the motion of multibody systems is the presence of high geometric nonlinearities. Therefore, appropriate analytical formalism and numerical procedures are necessary for obtaining reliable computer simulations of the dynamic behavior of interest [43]–[45].

Several recent research works are devoted to the virtual prototyping of EVs. In particular, integrated multibody simulations of control systems with a full-vehicle dynamic model based on electrical systems can be found in the literature [46]–[48]. To obtain a general overview of electric vehicles, one can consult the journal paper [49], which illustrates the most used technologies, comparing the models on the market with the impact of electric vehicles on the environment, the economy, and the electricity grid. The theme of the impact of electric vehicles is dealt with in the detailed paper [50], in which the in-depth analysis proposed concerns vehicles of category L in general. For the study of vehicle performance, an excellent reference is the vehicle dynamics textbook by Guiggiani [51]. Also, useful references are the journal publications [52], [53], in which the half-body model of an electric vehicle is analyzed in particular. The longitudinal tire model developed using Pacejka's well-known Magic Formula described in the book [54] is useful for realistically describing the interaction between the tires and the ground also in the case of EVs. Furthermore, as far as the vehicle models developed in Matlab/Simulink is concerned, the reference papers [55]–[57] are recommended. For a review on the electrical motor drivelines in electric vehicles, the literature survey [58] is exhaustive. The suspension system suitable for the vehicle of category L7 considered in this work are studied also in the journal paper [59]. Azman et al. proposed a dynamic model that combines rebound, pitch, and roll to understand the overall behavior of the vehicle [60]. Tanik and Parlaktas adopted systematic approaches for the design and production of a class L7 electric vehicle [61]. In the publication [62], the different types of engines that are candidates for use in electric vehicles were analyzed. Yang et al. worked on the state of the art of electric and commercial propulsion systems in the north American automotive industry [63]. Albinson and Routledge proposed a Simulink model that simulates the behavior of a vehicle suspension [64]. Di Martino devised dynamic vehicle models in Matlab-Simulink, one with front-wheel drive and one with rear-wheel drive [65]. Nair and Rajagopal proposed a Matlab-Simulink model that simulates the entire vehicle dynamics [66]. Lin et al. created a hybrid electric vehicle model in the Matlab-Simulink environment useful for the study of the energy management [67]. Mohd et al. developed a mathematical model for energy recovery and regeneration [68]. Lee et al. modeled and evaluated a power system model [69]. Xiaoling et al. constructed a hybrid model with parallel propulsion [70]. Tabbache et al. proposed an adaptive electric differential system for an electric vehicle with two induction motors [71]. Gao et al. proposed a hybrid electric vehicle model [72]. Kroeze and Kerin designed a battery model in dynamic simulations of electric vehicles [73]. McDonald presented the simulation of a basic electric vehicle driving system that is used to study power flow during both motorization and regeneration [74]. The book by Ehsani et al. is an introduction to vehicle technologies, with details of hybrid, electric, and fuel cell vehicles [75]. The large number of research works reported before is focused on the different aspects concerning the modeling and prototyping of EVs and demonstrates the importance of the topics investigated in this paper.

D. Scope and Contributions

The main goal of this investigation is the development of a mathematical model of a new electric vehicle of class L7 in order to predict the fuel consumption and optimize the performance of the ground vehicle. For this purpose, a model-based system engineering approach is employed and a virtual model of the engineering system of interest is designed by using the Simscape tool of Matlab that allows for constructing dynamical models of physical systems within the Simulink environment. According to the subdivision in vehicle categories established by the United Nations Economic Commission for Europe (UNECE), L7 vehicles are four-wheel vehicles having an unloaded mass lower than 400 kg, excluding the weight of the batteries in the case of electric vehicles, and with a maximum continuous rated power lower than 15 kW.

In this preliminary study, a simple mechanical model is employed for readily modeling the dynamics of the vehicle of interest. To this end, a half-car vehicle model was formulated and used in this work taking into account the main phenomena relevant for the present analysis. The dynamical model considered includes three degrees of freedom that are the vehicle longitudinal displacement (cruise), the vehicle vertical displacement (bounce), and the vehicle angular displacement about a transversal axis (pitch). The principal forces and moments that affect the vehicle dynamics are included in the mechanical model, such as the elastic and viscous forces associated with the suspension system as well as the generalized forces generated by the contact between the tires and the ground. In particular, the tires are modeled considering an equivalent set of stiffness and damping coefficients and also considering the Magic Formula of Pacejka. Furthermore, three different configurations are considered in this work for modeling the powertrain. In the first configuration, a central electric engine having a fixed gear ratio is considered. In this configuration, a differential gear train is used to transmit the driving torque to the wheels. The second configuration considered is indeed similar to the first configuration and includes also a transmission system that realizes two gear ratios for varying the vehicle velocity. The last configuration for the powertrain is different from the previous two standard ones. In the third configuration, two independent electric motors are considered and are collocated on the two driving wheels of the vehicle. In this case, similarly to the first configuration, the speed ratio cannot be changed. These three specific design configurations assumed for the electric vehicle of interest are based on engineering considerations related to the subsequent practical feasibility

of the virtual prototype which will be addressed in future research works.

For the three configurations of the powertrain considered in this study, the ground propulsion system is composed of a Permanent-Magnet Synchronous Motor (PMSM), a power supply made with lithium batteries, and a closed-loop control system for the torque control. The closed-loop control system used for the electric motor is programmed considering three different scenarios. In the first scenario, an arbitrary set of time functions generated by the driver is imposed in input to the electric motor. In the second scenario, a cruise-control system is considered and, therefore, a constant forward velocity is maintained by the controller. The last scenario programmed for the feedback controller is based on a pre-established driving cycle. The cruise control and the controller for the driving cycle are realized considering a Proportional-Integral (PI) controller based on the error between the actual velocity of the vehicle obtained using the dynamical model and the prescribed velocity associated with the standard driving cycle considered as the target. These various scenarios are considered in order to perform a comparison between the different design configurations of interest for this research study. For this purpose, a useful comparative analysis can be performed in the virtual prototyping phase of the mechanical design for obtaining an optimal design of the new vehicle. The systematic comparison performed in this work is based on the numerical results obtained by using the virtual prototype developed in the Matlab-Simulink environment.

E. Manuscript Organization

The remaining part of this paper is structured as follows. In Section II, the background materials and the computational methods employed in this research work are described. Section III proposes the developments and the design solutions for the virtual prototype of the electric vehicle of category L7 that represents the main object of the present paper. In Section IV, the numerical results found in this investigation are reported and a comparative discussion on three design configurations is provided. Section V offers a summary of the work, the conclusions reached in this paper, and some viable directions of future research.

II. Background Materials and Computational Methods

In the development of the present work, a systematic approach based on a system engineering strategy is used. Firstly, the main object of study is examined, thereby analyzing the various existing components for EVs, such as batteries, charging stations, engines, and the different possible configurations. Subsequently, for the creation of the mathematical model in a virtual environment, a systematic approach is employed, dividing the whole system into simpler problems. Once solved the individual problems, the complete system is assembled creating a general electromechanical vehicle model. From the basic features of the dynamical model, three different L7 vehicle configurations are created in order to perform a general comparison. In this section, the Matlab-Simulink environment and the Simscape libraries employed for developing the virtual prototype of the electric vehicle of interest are described together with the standard driving cycles used for assessing the performance of the vehicle design configurations devised in this work.

A. Matlab-Simulink Environment and Simscape Libraries

For the development of the virtual prototype of the vehicle model considered in this investigation, the Matlab/Simulink software was used. In particular, an application included in the Matlab calculation program was employed, which constitutes, in large part, a powerful and intuitive graphic interface aimed at simplifying the model implementation by the user. Using Simulink it is possible to program the execution of calculations in the Matlab environment in a much faster and error-free way compared to the writing of the long and complex m-files that are necessary, for example, to program the numerical integration of a system of high-order differential-algebraic equations. Through the visual tools available in the Simulink environment, it is possible to simulate very complex systems with an effort by the user that is limited to the tracking, on an electronic worksheet, of a block diagram representative of the system under examination. Simulink consists of a series of libraries that contain elementary blocks, which, properly interconnected, form the block diagram representing the desired functionality. The particular set of libraries used to conduct the present study is Simscape, in which the blocks represent physical elements having different levels of fidelity relative to the different levels of the system being analyzed. The lines which connect these components correspond to physical connections in the real system aimed at realizing the power transmission. This method thus allows for graphically describing the physical structure of the system of interest rather than the underlying mathematical models. The electrical, mechanical, and thermal connections are represented by different colors that indicate their physical domains. This software was used in this research work to carry out preliminary simulations of the dynamical behavior of the electric vehicle in a more economical and efficient way compared to hardware prototypes.

B. Standard Driving Cycles

To evaluate the performance of different design configurations, it is necessary to define the conditions of the trajectory and the driving cycle. There are three types of driving cycles considered in the automotive industry: (a) urban; (b) extra-urban; and (c) mixed. The first is characterized by low speeds, frequent accelerations and decelerations, and long periods during which the vehicle is stationary but the engine is still in operation. The second involves higher peak speeds and more regular driving, thus simulating the travel of secondary roads and/or highways. Finally, the third type, the mixed one, includes the combined set of the other two. Different driving cycles have been developed by different institutions. The purpose of the driving cycles is to avoid ambiguity in performance evaluation and to provide a unique means of comparison. In this way, vehicles with different characteristics can be compared. Given the power of the vehicle studied, reference is made to cycles for light vehicles. In particular, the WLTP (Worldwide harmonized Light vehicles Test Procedure) cycle was chosen in this work for the dynamic tests. It is the equivalent of the NEDC (New

European Driving Cycle) but is developed by international bodies including the European Union, Japanese, and Indian commissions. The choice to introduce this cycle is motivated by the desire to create a profile that is closer to the real driving style used with light vehicles for transporting people. In fact, the NEDC cycle, having been introduced in the seventies, does not take into account the development of cars in subsequent years. The increase in available power translates into a considerable increase in the acceleration values of the vehicles: it has gone from an average of 14 seconds to an average of 10 to go from 0 to $100\,\mathrm{km/h}$. As a result, today, we have a much more aggressive and irregular driving style with greater acceleration and deceleration. The objective of the WLTP is mainly to obtain a model more faithful to the current driving styles and, consequently, to prevent the manufacturers from optimizing the engine mapping based on the test cycle: this, in fact, would allow the manufacturer to obtain excellent efficiency results in the trials, but without guaranteeing an equally important outcome in a real driving session. The standard WLTP cycle, being an international model that must take into account a large variety of vehicle types, is divided into three different categories of cycles which are classified according to the Power/Weight (kW/t) ratio indicated with PW according to the following criteria:

- Class 1: Vehicles having $\mathrm{PW} < 22$ (kW/t);
- Class 2: Vehicles having $22 \leq \mathrm{PW} \leq 34$ (kW/t);
- Class 3: Vehicles having $\mathrm{PW} > 34$ (kW/t);

Given the reduced motor power in the developed models, reference is made to the WLTP Class 1 cycle, of which the velocity and acceleration profile is shown in Figure 1.

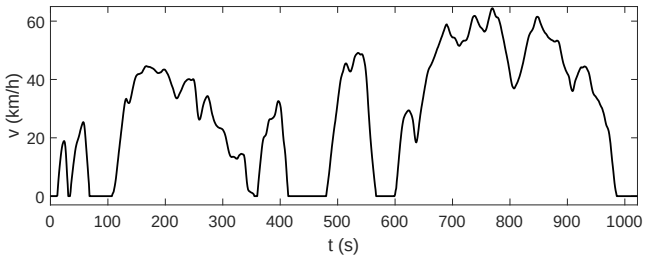

(a) Velocity.

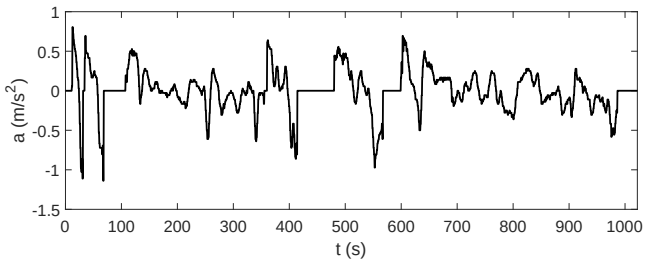

(b) Acceleration.

Fig. 1. Velocity and acceleration of the WLTP cycle of class 1.

Figures 1(a) and 1(b) respectively show the velocity and the acceleration of the WLTP cycle assumed in this investigation for testing the dynamic and electric performance of the electric vehicle designed in this work considering the three different configurations discussed before.

III. Electric Vehicle Virtual Prototype

In this section, the component models that form the virtual prototype of the electric vehicle are illustrated in detail. To this end, a Matlab/Simulink model is created by using a standard design configuration for the electric vehicle as the starting point. A CAD geometric model of the virtual prototype of the electric vehicle of class L7 of interest for this investigation is represented in Figure 2.

Fig. 2. CAD model of the electric vehicle of class L7.

The initial design configuration for the virtual model of the electric vehicle can be divided into four macrosystems interconnected with each other. The four macrosystems are: 1) the electrical system, 2) the thermal system, 3) the control system, and 4) the vehicle mechanical system. In particular, the vehicle mechanical system is described in detail including a) the half-car dynamic model, b) the tires model, c) the brakes model, d) the mechanical differential model, and e) the clutch and gearbox models. The final aim of the system engineering approach employed in this study is the improvement of the dynamic and control apparatus, for finally creating three different vehicle configurations. The subsystems that form the complete model of the electric vehicle of class L7 are described below.

A. Electric System

In this subsection, the electric subsystem is described. The electrical system is powered by a lithium-ion battery consisting of 10 parallels composed of 50 series of cells each. The equivalent circuit of the cell has been created as shown in Figure 3.

As shown in Figure 3, the battery model has as outputs the positive and negative connection of the circuit and the heat generated by the batteries. This subsystem is composed of a resistance in parallel with a capacitor and another resistance. Battery performance is also influenced by temperature, as discussed in the next subsection. In the battery equivalent model, the cell voltage is modeled as:

$$V(t) = E(t) - V_C(t) - i(t)R_0 \tag{1}$$

or equivalently:

$$V(t) = E(t) - R_1 i_{R_1}(t) - i(t)R_0 \tag{2}$$

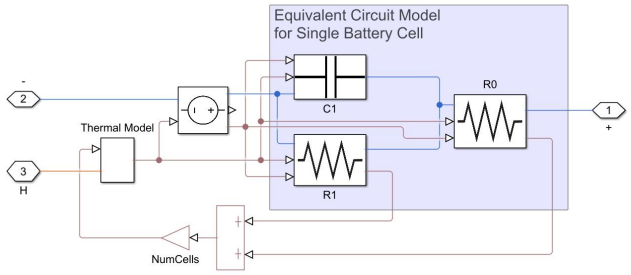

Fig. 3. Battery cell equivalent circuit.

where $V(t)$ is the voltage of a parallel of cells, $E(t)$ is the voltage generated from a parallel of cells, whereas R_0, R_1, and C depend on the temperature of the cell according to tabled values. To find an expression for the $i_{R_1}(t)$, one should recognize that the current through R_1 plus the current through C is $i(t)$. Assuming:

$$i_{C_1}(t) = C_1 \dot{V}_C(t), \quad V_c(t) = R_1 i_{R_1}(t) \tag{3}$$

One obtains:

$$i(t) = C_1 \dot{V}_C(t) + i_{R_1}(t) \tag{4}$$

Consequently, the differential equation that should be integrated to determine $i_{R_1}(t)$ is given by:

$$i_{R_1}(t) + R_1 C_1 \frac{di_{R_1}(t)}{dt} = i(t) \tag{5}$$

or:

$$\frac{di_{R_1}(t)}{dt} = -\frac{1}{R_1 C_1} i_{R_1}(t) + \frac{1}{R_1 C_1} i(t) \tag{6}$$

By multiplying the voltage obtained from a series of cells by the number of cells connected in series, the battery voltage is obtained. The main characteristics of the batteries used in the model of the electric vehicle are reported in Table I.

TABLE I
BATTERY DATA.

Battery	Data	Units
Battery technology	Lithium-ion	–
Cells in series	50	–
Parallel of cells in series	10	–
Deficit of initial cell charge	15.65	Ah
Cell initial temperature	293	K

There is a DC-DC converter to transform the current from the battery voltage to the motor voltage. The electric motor is synchronous with permanent magnets with closed-loop torque control, which means that the input voltage and power adjust according to the torque required by the control system. Therefore, having at the motor input the electric current, regulated by the controller, the rotation of the rotor and the heat generated are obtained in output. Furthermore, in the case of negative torque and positive speed, the electric machine operates like a current generator recharging the batteries. This property is exploited in the virtual prototype of the electric vehicle as discussed hereafter. The Matlab/Simulink block of the electric engine used is represented in Figure 4.

As shown in Figure 4, the motor model has as inputs the torque required by the controller, the electrical connection,

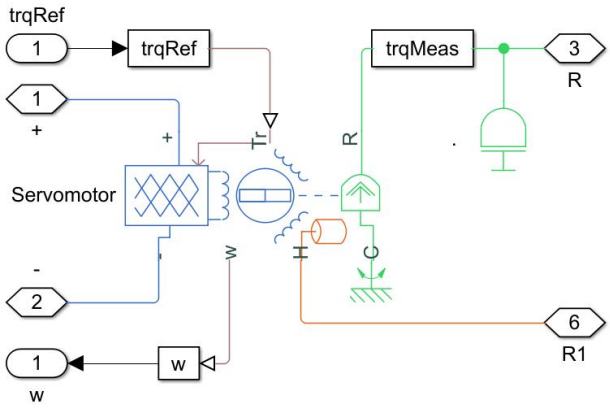

Fig. 4. Electric motor.

the rotation of the rotor, and the heat generated by the motor. The main characteristics of the electric engine are reported in Table II.

TABLE II
ELECTRIC ENGINE DATA.

Motor	Configurations 1-2	Configuration 3	Units
Max torque	83	44	Nm
Max power	13	6.9	kW
Max efficiency	96	96	%
Max Speed	1500	1500	rpm
Motor inertia	0.0048	0.026	kg × m^2

These data complete the description of the electric system.

B. Thermal System

In this subsection, the thermal subsystem is described. The thermal model is divided into two parts, namely the convective exchange system between the batteries and the environment, and the liquid cooling system for the engine. In the first subsystem, the thermal power generated by the batteries is that dissipated by the resistance of the equivalent circuit, and therefore, to obtain the heat exchanged in a convective way with the environment, it is necessary to provide the specific mass and heat of the batteries. On the other hand, the second system is a thermodynamic water cycle which is composed of a radiator that transfers heat to the environment, a pump that allows the recirculation of the liquid, the engine that supplies heat to the system, and an expansion vessel (expansion tank) which allows to contain sudden pressure variations avoiding rushes and water hammering. The radiator is schematized by tubes with a fixed volume of liquid, which loses pressure due to viscous friction, according to the Darcy-Weisbach law, and gives heat to the environment through the walls, following the correlation with the Nusselt number. The same principles are applied to the engine which, on the contrary, supplies heat to the vehicle system. In general, the convective heat exchange is described by the following equation:

$$\dot{Q} = kA(T_{ENV} - T_B) \tag{7}$$

where $\dot{Q}$ is the heat flow, k is the convection heat transfer coefficient, A the exchange surface area, T_{ENV} the environment temperature, and T_B the battery temperature. The heat

flow rate between the thermal liquid and the pipe wall can be obtained as follows:

$$\dot{Q}_H = \dot{Q}_{conv} + \frac{k_I A_H}{D}(T_H - T_I) \tag{8}$$

where $\dot{Q}_H$ is the net heat flow rate, $\dot{Q}_{conv}$ is the portion of the heat flow rate attributed to convection, k_I is the thermal conductivity of the liquid at the internal fluid volume of the pipe, A_H is the surface area of the pipe wall, namely the product of the pipe perimeter and length, T_H and T_I are the temperatures at the pipe wall and at the internal fluid volume of the pipe. In particular, the convective heat flow is given by:

$$\dot{Q}_{conv} = \dot{m} c_p (T_H - T_{in}) \left(1 - e^{-\frac{hA_H}{\dot{m}c_p}}\right) \tag{9}$$

where $\dot{m}$ is the mass flow rate, c_p is the specific heat coefficient, and T_{in} is the inlet temperature. In addition, the heat transfer coefficient denoted with h depends on the Nusselt number as follows:

$$h = Nu\frac{k_I}{D} \tag{10}$$

where the Nusselt number is defined as:

$$Nu = \frac{\frac{f}{8}(Re - 1000)\,Pr}{1 + 12.7\sqrt{\frac{f}{8}}\left(Pr^{2/3} - 1\right)} \tag{11}$$

where f is the Darcy friction factor, Re is the Reynolds number, and Pr is the Prandtl number evaluated at the average temperature. The Reynolds number is computed as follows:

$$Re = \frac{\dot{m}D}{A\mu} \tag{12}$$

where μ is the dynamic viscosity at the average temperature, D is the diameter of the pipe, and A the surface area. The scheme of the water cooling system is reported in Figure 5.

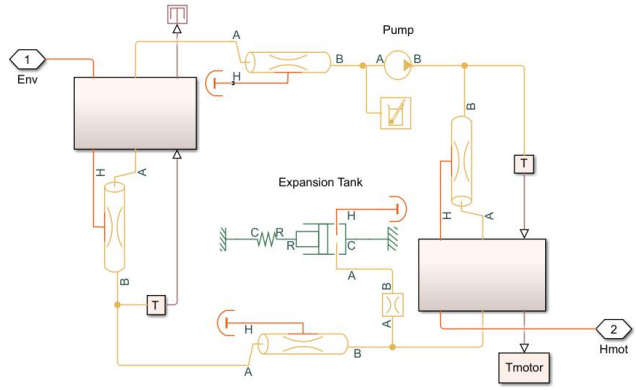

Fig. 5. Water cooling system.

As shown in Figure 5, the cooling system has as input the heat exchanged with the motor and has as output the heat exchanged with the environment. The main characteristics of the thermal system are reported in Table III.

These data complete the description of the thermal system.

TABLE III
THERMAL SYSTEM DATA.

Thermal System	Data	Units
Cell area	0.1019	m^2
Pipe radiator length	2000	mm
Pipe exchanger length	400	mm
Hydraulic diameter	50	mm
Cross-sectional area	1964	mm^2
Darcy friction factor	64	–
Mass flow rate	20	kg/s

C. Control System

In this subsection, the control subsystem is described. As already stated previously, the motor is controlled by requesting a certain driving torque to the controller, which must be less than the maximum torque that can be supplied and whose power must not exceed the maximum power available. The calculation of this torque takes place according to three different methods: (a) by responding to the driver's input; (b) using the cruise control; or (c) by having the vehicle to follow a driving cycle. The control system is schematically represented in Figure 6.

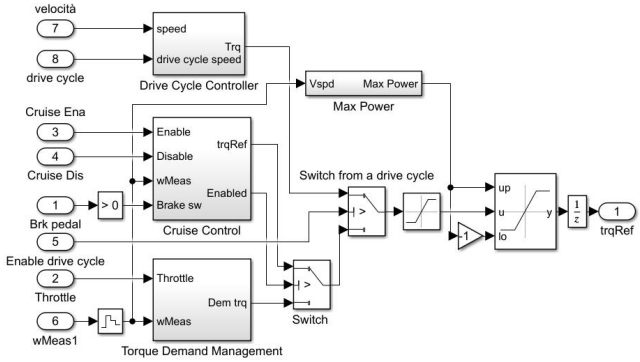

Fig. 6. Control system.

The three alternative methods used for the determination of the driving torque in the model of the control system applied to the electric vehicle are described in detail below.

1) Driver Input: This control system is of the open-loop type. The required torque is obtained based on the driver input supplied to the system by means of a prescribed time law which indicates the accelerator pedal percentage as a function of time. In the case of zero pedal percentage and with a positive speed, the motor is asked for a negative torque, making it work as a current generator, for example using the regenerative braking strategy, as can be seen in Figure 7.

As shown in Figure 7, the control system has as inputs the accelerator signal in the open loop and the engine speed, resulting as the output the torque to be provided to the engine. In this dynamical system, the following control law is used:

$$\begin{cases} T = \frac{\alpha}{100} T_{\max}, & \alpha > 0, \quad \omega > 0 \\ T = -T_{\max}, & \alpha = 0, \quad \omega > 0 \\ T = 0, & \alpha = 0, \quad \omega \leq 0 \end{cases} \tag{13}$$

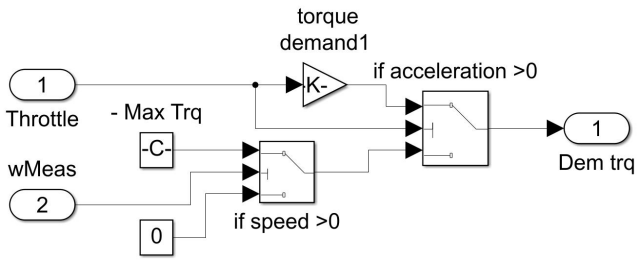

Fig. 7. Open loop controller.

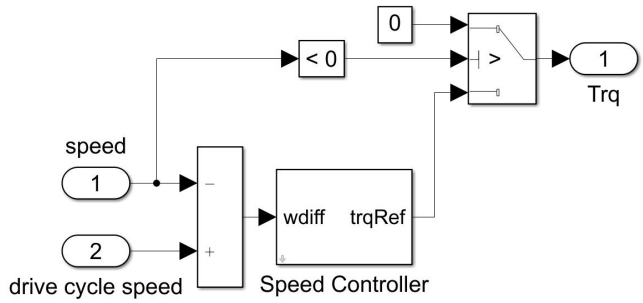

Fig. 9. Driving cycle control.

where T is the effective torque, T_{max} is the maximum torque, α is the percentage throttle angle, and ω is the engine angular velocity.

2) Cruise Control: Using a proportional and integrative closed-loop control scheme, the vehicle is induced to follow a reference speed. This feedback control system is activated by supplying the "Enable" Boolean command by means of a graph as a function of time and can be deactivated both in the event of braking and in the event of a "Disable" command. The angular speed of reference, captured at the time of activation, is compared with the angular speed at the motor output, obtaining as the controller output the torque to be requested from the motor. In Figure 8, the Simulink model of the cruise control is presented.

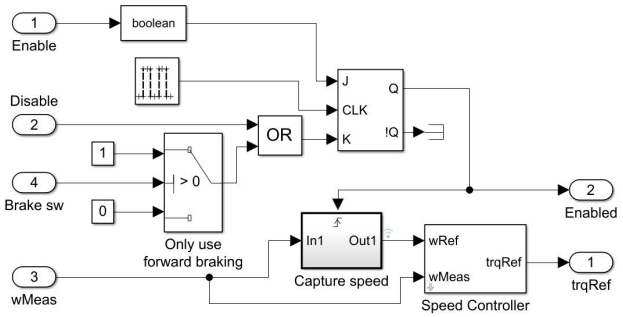

Fig. 8. Cruise control.

As shown in Figure 8, the cruise control system has as input the cruise control activation signal, the deactivation signal, the braking signal, and the engine speed. The output obtained is the torque requested at the engine.

3) Driving Cycle Time Law: A driving cycle is used to compare the three vehicle configurations and to obtain tests that represent typical driving conditions on urban roads. For this purpose, the WLTP cycle of class 1 is used. Considering a control architecture in closed-loop of proportional and integrative type, the vehicle follows the speed required by the driving cycle, provided by the special control block devised to this end. This feedback control scheme compares the actual speed of the vehicle with the target velocity, thus obtaining from the controller the torque necessary for the engine. In Figure 9, the Simulink model of the system driving controller is presented.

As shown in Figure 9, the control system has as input the vehicle's velocity and the driving cycle's velocity, while the output obtained is the torque requested at the engine.

D. Vehicle Mechanical System

In this subsection, the mechanical model of the electric vehicle is described. The mechanical parts of the electric vehicle of interest are modeled considering a simplified multibody approach [76], [77]. To this end, the mechanical model of the dynamical system is based on a half-car vehicle model with three degrees of freedom: the forward displacement (advancement), the vertical displacement (bouncing), and the transverse angular displacement (pitch). In order to consider the different forces acting on the ground vehicle, such as the aerodynamic resistance induced by the air flow as well as the restoring elastic forces due to the suspensions and viscous damping forces induced by the shock absorbers, the three degrees of freedom considered are coupled with two additional vertical displacements that model the motion of the wheels [78]. The behavior of the tires is also taken into account using the well-known Magic Formula of Pacejka and considering the linear approximation for the tire stiffness and damping coefficients [79]. The propulsion unit has been modeled according to three different configurations: (I) the first consists of a central engine, with a fixed transmission ratio and a mechanical differential that distributes the driving torque to the wheels [80]; (II) the second configuration is similar to the previous one but is equipped with a two-speed gearbox; and finally, (III) the third configuration is composed of two motors in parallel, one for each driving wheel, with a fixed transmission ratio. The three design configurations considered for the mechanical model of the electric vehicle are illustrated in detail below.

1) Design Configuration 1: In the first configuration, the rotation obtained by the motor is first reduced by a fixed gear, then distributed by a mechanical differential to the two driving wheels. By using this transmission system, the longitudinal force which affects the dynamic model acting on the axis of the wheels is calculated. In electric vehicles, it is possible not to use the speed change, since the electric motors, compared to traditional internal combustion engines, have a high starting torque, much higher maximum revolutions per minutes, and good efficiency for a wide speed range. In Figure 10, the scheme of the first design configuration is presented.

Figure 11 shows the Matlab/Simulink model of the design of the first configuration.

2) Design Configuration 2: The second configuration is very similar to the first design but, instead of having a fixed gearbox, there is a two-speed gearbox controlled by a switch that changes gear depending on the speed of the vehicle. In

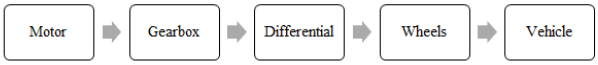

Fig. 10. Scheme of the design configuration 1.

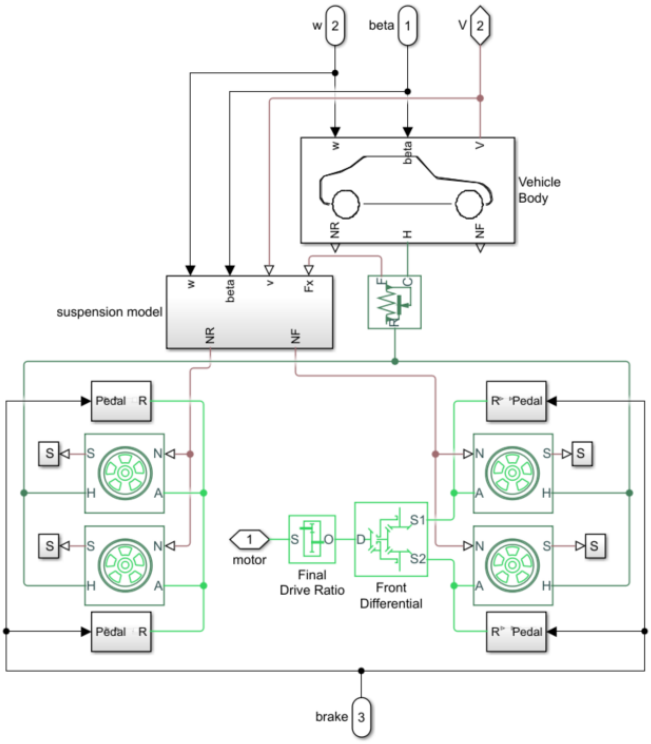

Fig. 11. Matlab/Simulink model of the design configuration 1.

Figure 12, the scheme of the second design configuration is presented.

Fig. 12. Scheme of the design configuration 2.

Figure 13 shows the Matlab/Simulink model of the design of the second configuration.

3) Design Configuration 3: The third and last configuration consists of two electric motors connected in parallel, each of which provides its torque to the driving wheels, connected via a fixed transmission ratio. In Figure 14, the scheme of the third design configuration is presented.

Figure 15 shows the Matlab/Simulink model of the design of the third configuration.

In Figure 16, the electric motors working in parallel in the third design configuration are shown.

These data complete the description of the vehicle mechanical model and its three design configurations.

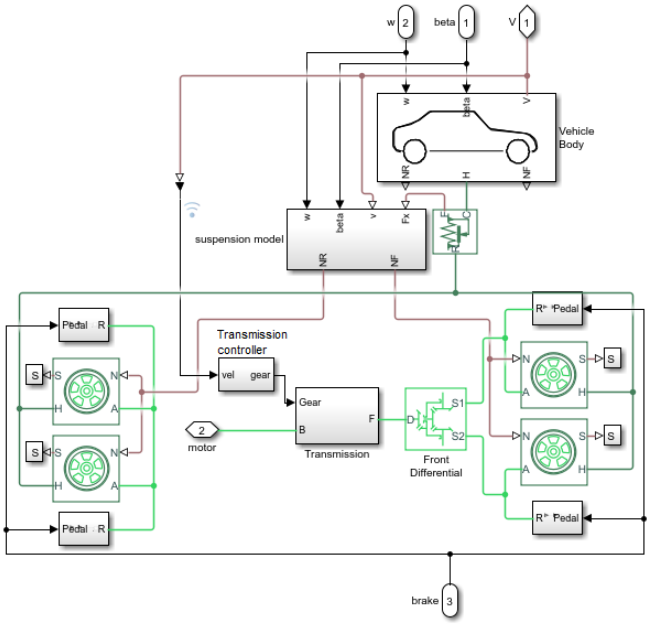

Fig. 13. Matlab/Simulink model of the design configuration 2.

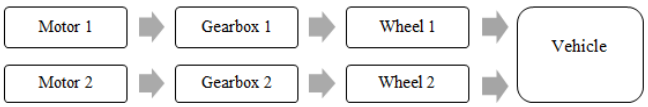

Fig. 14. Scheme of the design configuration 3.

E. Half-Car Dynamic Model

In this subsection, the mechanical model employed for describing the longitudinal and vertical dynamics of the electric vehicle is described. The mechanical model developed in this subsection represents the fundamental dynamical model used for optimizing the performance of the virtual prototype of the electric vehicle that is the main object of this investigation. To this end, a nonlinear dynamic half-car model with three degrees of freedom is used. The principal degrees of freedom are the advancement, the bounce, and the pitch. Other two displacement degrees of freedom are also added to the basic set of three generalized coordinates, giving the possibility of including the stiffness and damping effects of the tires. Thus, the dynamical model of the electric vehicle is based on a total of $n = 5$ generalized coordinates grouped in the column vector denoted with $\mathbf{q}$ and given by:

$$\mathbf{q} = \begin{bmatrix} x & z & \theta & z_1 & z_2 \end{bmatrix}^T \tag{14}$$

where x is the chassis forward displacement, z is the chassis vertical displacement, θ is the chassis angular displacement, and z_1 and z_2 are respectively the vertical displacements of the front and rear wheels labeled with the numbers 1 and 2. Figure 17 shows the scheme of the dynamical model used for the electric vehicle.

Since a minimal set of generalized coordinates is employed for describing the kinematics of the electric vehicle, the dynamic equations can be obtained by the direct application of the Lagrange equations of the second kind given

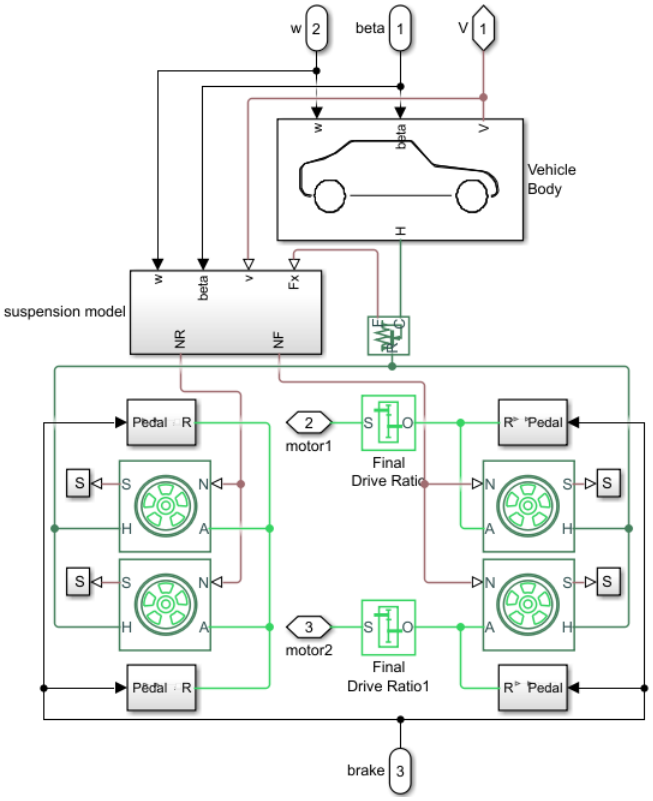

Fig. 15. Matlab/Simulink model of the design configuration 3.

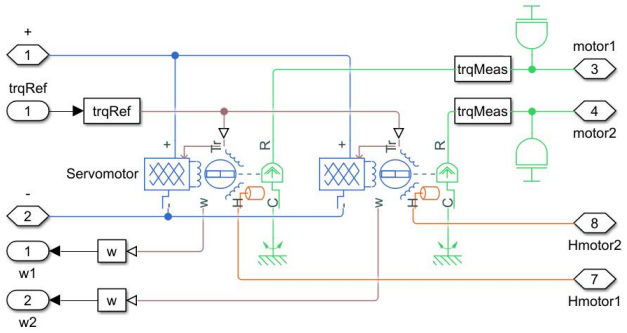

Fig. 16. Electric motors working in parallel.

by:

$$\frac{d}{dt}\left(\frac{\partial T}{\partial \dot{\mathbf{q}}}\right)^T - \left(\frac{\partial T}{\partial \mathbf{q}}\right)^T + \left(\frac{\partial R}{\partial \dot{\mathbf{q}}}\right)^T + \left(\frac{\partial U}{\partial \mathbf{q}}\right)^T = \bar{\mathbf{Q}}_{e,nc} \quad (15)$$

where T is the total kinetic energy of the system inertial components, R is the total Rayleigh dissipation function associated with the dissipative force fields applied on the mechanical system, U is the total potential energy relative to the conservative force fields acting on the dynamical system, and $\bar{\mathbf{Q}}_{e,nc}$ is the total generalized force vector arising from the external actions induced by the presence of the force fields that cannot be expressed as the derivative of a given scalar function. By manipulating the Lagrange equations of the second time, one can prove that [2]:

$$\frac{d}{dt}\left(\frac{\partial T}{\partial \dot{\mathbf{q}}}\right)^T - \left(\frac{\partial T}{\partial \mathbf{q}}\right)^T = \mathbf{M}\ddot{\mathbf{q}} - \mathbf{Q}_v \quad (16)$$

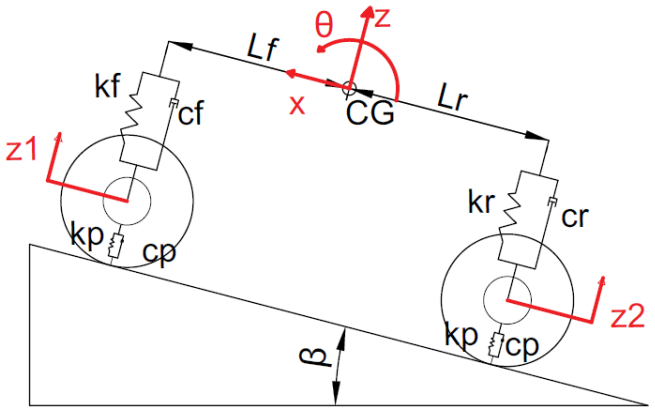

Fig. 17. Scheme of the dynamical model.

and

$$\mathbf{Q}_{e,nc} = \bar{\mathbf{Q}}_{e,nc} - \left(\frac{\partial R}{\partial \dot{\mathbf{q}}}\right)^T, \quad \mathbf{Q}_{e,c} = -\left(\frac{\partial U}{\partial \mathbf{q}}\right)^T \quad (17)$$

where $\mathbf{q}$, $\dot{\mathbf{q}}$, and $\ddot{\mathbf{q}}$ respectively denote the system generalized position, velocity, and acceleration vectors, $\mathbf{M} = \mathbf{M}(\mathbf{q}, t)$ identifies the system mass matrix, $\mathbf{Q}_v = \mathbf{Q}_v(\mathbf{q}, \dot{\mathbf{q}}, t)$ is the inertial generalized force vector that absorbs the generalized force terms which are quadratic in the generalized velocities, while $\mathbf{Q}_{e,c} = \mathbf{Q}_{e,c}(\mathbf{q}, t)$ and $\mathbf{Q}_{e,nc} = \mathbf{Q}_{e,nc}(\mathbf{q}, \dot{\mathbf{q}}, t)$ respectively identify the total conservative and non-conservative generalized force vectors. For simplicity, one can also define:

$$\mathbf{Q} = \mathbf{Q}_v + \mathbf{Q}_{e,c} + \mathbf{Q}_{e,nc} \quad (18)$$

where $\mathbf{Q} = \mathbf{Q}(\mathbf{q}, \dot{\mathbf{q}}, t)$ represents the total generalized force vector acting on the mechanical system of interest. The dynamic model resulting from the implementation of the Lagrange equations of the second kind in the case of the half-car electric vehicle model is described by the following coupled set of nonlinear ordinary differential equations:

$$\begin{cases} m_c\ddot{x} = F_x - F_{a,x} - F_{g,x} \\ m_c\ddot{z} = F_{a,z} + F_{s,f} + F_{s,r} + F_{g,z} \\ I_{c,yy}\ddot{\theta} = -L_f F_{s,f} + L_r F_{s,r} + HF_x - M_{a,y} \\ m_w\ddot{z}_1 = -F_{s,f} + F_{p,1} \\ m_w\ddot{z}_2 = -F_{s,r} + F_{p,2} \end{cases} \quad (19)$$

where m_c is them mass of the chassis, $I_{c,yy}$ is the transverse mass moment of inertia of the chassis, m_w is the mass of each wheel, F_x is the longitudinal force applied on the wheel axis, $F_{a,x}$, $F_{a,z}$, and $M_{a,y}$ are respectively the longitudinal aerodynamic force, the vertical aerodynamic force, and the aerodynamic moment, $F_{s,f}$ and $F_{s,r}$ are respectively the elastic and damping force of the front and rear axle suspensions, $F_{g,x}$ and $F_{g,z}$ are respectively the longitudinal and vertical components of the gravity force, $F_{p,1}$ and $F_{p,2}$ are the total normal elastic and damping forces due to the tires respectively associated with the wheels 1 and 2, L_f and L_r are respectively the longitudinal distances from the center of mass CG to the front and rear axle, and H is the normal

distance between the center of mass CG and the wheel axes. The dissipative forces arising from the interaction between the air and the vehicle are directly proportional to the square of the difference between vehicle speed and wind speed as shown as follows:

$$\begin{cases} F_{a,x} = \frac{1}{2} C_d \rho A (\dot{x} - w)^2 \\ F_{a,z} = \frac{1}{2} C_l \rho A (\dot{x} - w)^2 \\ M_{a,y} = \frac{1}{2} C_m \rho A L (\dot{x} - w)^2 \end{cases} \tag{20}$$

where ρ is the air mass density, w is the air velocity, $\dot{x}$ is the vehicle forward velocity, A is the area of the vehicle cross section, $L = L_r + L_f$ is the vehicle total length, C_d is the aerodynamic drag coefficient, C_l is the aerodynamic lift coefficient, and C_m is the aerodynamic coefficient associated with the pitching moment. The elastic and damping forces of the suspension system are given by the following equations:

$$\begin{cases} F_{s,f} = -2k_f \left(z - z_1 - L_f \theta\right) \\ \qquad\quad - 2c_f \left(\dot{z} - \dot{z}_1 - L_f \dot{\theta}\right) \\ F_{s,r} = -2k_r \left(z - z_2 + L_r \theta\right) \\ \qquad -2c_r \left(\dot{z} - \dot{z}_2 + L_r \dot{\theta}\right) \end{cases} \tag{21}$$

where the multiplicative factors of two take into account the parallel configuration of the spring and damper elements associated with the rear and front suspensions, while k_f and c_f respectively denote the elastic stiffness and viscous damping coefficients of the front suspensions, whereas k_r and c_r respectively identify the elastic stiffness and viscous damping coefficients of the rear suspensions. The normal elastic and damping forces due to the tires are given by:

$$\begin{cases} F_{p,1} = -k_p x_1 - c_p \dot{x}_1 \\ F_{p,2} = -k_p x_2 - c_p \dot{x}_2 \end{cases} \tag{22}$$

where k_p and c_p respectively represent the elastic stiffness and viscous damping coefficients associated with the vehicle tires. The components of the vehicle weight force vector are can be calculated as follows:

$$\begin{cases} F_{g,x} = m_c g \sin(\beta) \\ F_{g,z} = m_c g \cos(\beta) \end{cases} \tag{23}$$

Thus, the equations of motion of the half-car vehicle can be easily rewritten in the following matrix form:

$$\mathbf{M}\ddot{\mathbf{q}} = \mathbf{Q} \tag{24}$$

In the case of the present half-car dynamic model, the system mass matrix $\mathbf{M}$ is a constant diagonal matrix while the total generalized force vector $\mathbf{Q}$ is a highly nonlinear vector function of the generalized positions and velocity vectors $\mathbf{q}$ and $\dot{\mathbf{q}}$ respectively given by:

$$\mathbf{M} = \begin{bmatrix} m_c & 0 & 0 & 0 & 0 \\ 0 & m_c & 0 & 0 & 0 \\ 0 & 0 & I_{c,yy} & 0 & 0 \\ 0 & 0 & 0 & m_w & 0 \\ 0 & 0 & 0 & 0 & m_w \end{bmatrix} \tag{25}$$

and

$$\mathbf{Q} = \begin{bmatrix} F_x - F_{a,x} - F_{g,x} \\ F_{a,z} + F_{s,f} + F_{s,r} + F_{g,z} \\ -L_f F_{s,f} + L_r F_{s,r} + H F_x - M_{a,y} \\ -F_{s,f} + F_{p,1} \\ -F_{s,r} + F_{p,2} \end{bmatrix} \tag{26}$$

Since the system mass matrix $\mathbf{M}$ is a constant diagonal matrix with a full rank, the system generalized acceleration vector $\ddot{\mathbf{q}}$ can be explicitly obtained from the total generalized force vector $\mathbf{Q}$ as follows:

$$\ddot{\mathbf{q}} = \mathbf{M}^{-1}\mathbf{Q} \tag{27}$$

or:

$$\begin{bmatrix} \ddot{x} \\ \ddot{z} \\ \ddot{\theta} \\ \ddot{z}_1 \\ \ddot{z}_2 \end{bmatrix} = \begin{bmatrix} \frac{F_x - F_{a,x} - F_{g,x}}{m_c} \\ \frac{F_{a,z} + F_{s,f} + F_{s,r} + F_{g,z}}{m_c} \\ \frac{-L_f F_{s,f} + L_r F_{s,r} + H F_x - M_{a,y}}{I_{c,yy}} \\ \frac{-F_{s,f} + F_{p,1}}{m_w} \\ \frac{-F_{s,r} + F_{p,2}}{m_w} \end{bmatrix} \tag{28}$$

By doing so, one can readily introduce a state space representation for transforming the dynamic equations from the configuration space to the state space. For this purpose, define the system state vector as follows:

$$\mathbf{z} = \begin{bmatrix} \mathbf{z}_1 \\ \mathbf{z}_2 \end{bmatrix} = \begin{bmatrix} \mathbf{p} \\ \mathbf{v} \end{bmatrix} = \begin{bmatrix} \mathbf{q} \\ \dot{\mathbf{q}} \end{bmatrix} \tag{29}$$

where $\mathbf{p} = \mathbf{q}$ identifies the system generalize position vector and $\mathbf{v} = \dot{\mathbf{q}}$ represents the system generalized velocity vector. By coupling the identity $\dot{\mathbf{z}}_1 = \mathbf{z}_2$ with the n second-order equations of motion, one obtains $2n$ first-order ordinary differential equations that form the system state space model expressed as:

$$\dot{\mathbf{z}} = \mathbf{f} \tag{30}$$

where $\mathbf{f}$ is the system state function defined as follows:

$$\mathbf{f} = \begin{bmatrix} \mathbf{f}_1 \\ \mathbf{f}_2 \end{bmatrix} = \begin{bmatrix} \mathbf{v} \\ \mathbf{a} \end{bmatrix} = \begin{bmatrix} \dot{\mathbf{q}} \\ \ddot{\mathbf{q}} \end{bmatrix} \tag{31}$$

where $\mathbf{a} = \ddot{\mathbf{q}}$ represents the system generalized acceleration vector explicitly obtained previously. The representation of the equations of motion in the state space form is particularly convenient because it allows for the use of standard numerical integration subroutines that are optimized in terms of accuracy and distribution of the numerical solution on the time grid. In general, these are desirable features and are especially useful in the case of the construction of complex and multi-components dynamical models such as the vehicle model developed in this research work. The system equations of motion are coupled and, therefore, are solved with the use of specific Matlab-Simulink blocks. The numerical values used for the dynamical simulations refer to a generic vehicle of category L7. In particular, the damping and stiffness coefficients of the suspension, and of the tires, are those presented in the research work [60], in which a vehicle with a mass comparable to that chosen in the present research paper is analyzed. Table IV shows a comprehensive list of vehicle model data.

These data complete the description of the dynamical model of the electric vehicle.

TABLE IV
VEHICLE MODEL DATA.

Vehicle Properties	Data	Units
Vehicle mass	450	kg
Driver mass	70	kg
Frontal suspension damping	4000	$\mathrm{N \times s/m}$
Rear suspension damping	4000	$\mathrm{N \times s/m}$
Frontal suspension stiffness	35000	$\mathrm{N/m}$
Rear suspension stiffness	50000	$\mathrm{N/m}$
Mass moment of inertia	2100	$\mathrm{kg \times m^2}$
Distance CG-frontal axis	0.6	m
Distance CG-rear axis	0.4	m
Equilibrium axis height from CG	0.4	m
Drag coefficient	0.4	–
Lift coefficient	0.2	–
Pitching moment coefficient	0.3	–
Frontal area	1.5	$\mathrm{m^2}$

F. Tires Model

In this subsection, the subsystem describing the vehicle tires is presented. To model the tire using the Simulink package 'Tire Block (Magic Formula)', which describes the longitudinal dynamical behavior induced by the tires, an empirical formula based on four adaptation coefficients is employed. The block models the dynamics of the tire considering it as a rigid system assembled with the wheel, both in constant and variable road conditions, and evaluates its inertia, rolling resistance, and the slip coefficient denoted with κ. Moreover, this approach considers the stiffness and damping effects induced by the tire. The model used is based on the Pacejka's Magic Formula [54], whose parameters should be determined through experimental tests. Based on the Magic Formula, the forces applied on the tire are shown in Figure 18(a).

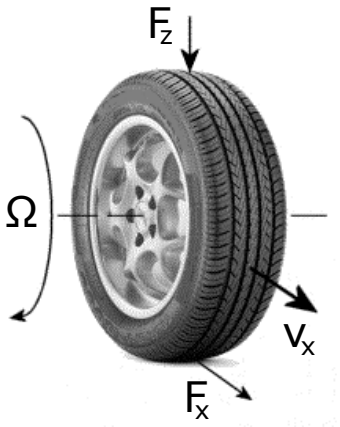

(a) Tire forces.

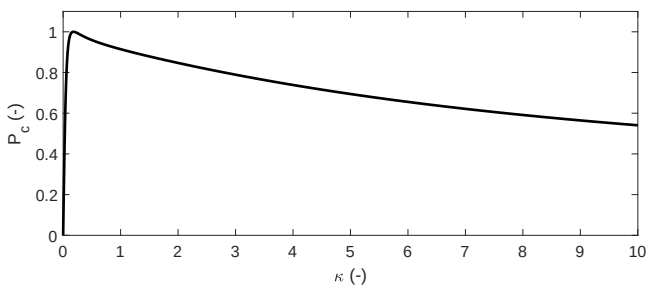

(b) Pacejka coefficient.

Fig. 18. Tire model.

In general, the longitudinal force denoted with F_x is given by the product between the Pacejka coefficient called P_c and the normal force indicated with F_z as follows:

$$F_x = P_c F_z \tag{32}$$

and

$$P_c = D \sin(\alpha_c) \tag{33}$$

where:

$$\begin{cases} \alpha_c = C \arctan(\beta_c) \\ \beta_c = \delta_c - E\gamma_c \\ \gamma_c = \delta_c - \arctan(\delta_c) \\ \delta_c = B\kappa \end{cases} \tag{34}$$

where the coefficients B, C, D, and E are obtained from the curve represented in Figure 18(b). This function passes through the origin of the Cartesian system, reaches a maximum, and then tends to a horizontal asymptote. The slip coefficient κ is given by the ratio between the velocity of slip and the forward velocity. Therefore, one can write:

$$\kappa = \frac{v_{s,x}}{|v_x|} = \frac{R_w \Omega - v_x}{|v_x|} \tag{35}$$

where $v_{s,x}$ is the computed slip velocity, $v_x = \dot{x}$ is the actual forward velocity, Ω is the angular velocity of the wheel, and R_w is the wheel radius. At low velocities, the Magic Formula does not appear to work properly for the dynamical model developed for the electric vehicle. In order to solve this problem, if the tire velocity is lower than a threshold speed, $|v_x| \leq |v_{th}|$, a numerical value that should be obtained through experimental testing, the equation used to calculate the slip coefficient is substituted with:

$$\kappa = \frac{2v_{s,x}}{v_{th} + \frac{v_x^2}{v_{th}}} \tag{36}$$

This equation is obtained experimentally and is proved to work properly for solving the problem at hand. This modification allows for a nonsingular nonzero slip at zero wheel velocity. For example, for perfect slipping, that is, in the case of a non-translating spinning tire, $v_x = 0$ while $\kappa = 2R_w\Omega/v_{th}$ is finite. The coefficients used for the tire model based on the Magic Formula of Pacejka are reported in Table V.

TABLE V
TIRE DATA.

Tire Properties	Data	Units
Coefficient B of the Magic Formula	10	–
Coefficient C of the Magic Formula	1.9	–
Coefficient D of the Magic Formula	1	–
Coefficient E of the Magic Formula	0.97	–
Tire radius	0.2	m
Tire stiffness	200000	$\mathrm{N/m}$
Tire damping	1000	$\mathrm{N \times s/m}$
Rolling resistance coefficient	0.015	–
Velocity threshold	0.001	$\mathrm{m/s}$

These data complete the description of the dynamic model used for the tires.

G. Brakes Model

In this subsection, the model of the brakes used for the electric vehicle is described. The model used considers the brake as a cylinder that applies pressure to a pad that generates friction with the brake disc, thus obtaining a resistant torque that opposes the rotation. The closing pressure is obtained on the basis of the driver inputs supplied to the system by means of a time law which indicates the percentage of the brake pedal denoted with β as a function of time. The equation used to calculate the braking torque is:

$$T_{br} = \frac{\mu_k P \pi {D_b}^2 R_m N}{4}, \quad \Omega \neq 0 \tag{37}$$

or:

$$T_{br} = \frac{\mu_s P \pi {D_b}^2 R_m N}{4}, \quad \Omega = 0 \tag{38}$$

where:

$$P = \frac{\beta}{100} P_{\max} \tag{39}$$

where T_{br} is the braking torque, P is the closing pressure, β is the percentage of closure of the pedal brake, Ω is the tire angular velocity, N is the number of pads in the brake caliper, μ_s is the static friction coefficient between the disk and the pad, μ_k is the dynamic friction coefficient between the disk and the pad, D_b is the diameter of the brake actuator, R_m is the nominal radius to which the force of the pad on the brake disc is applied, R_0 is the outer radius of the brake pad, and R_i is the inner radius of the brake pad. Figure 19 shows the scheme of the brake model.

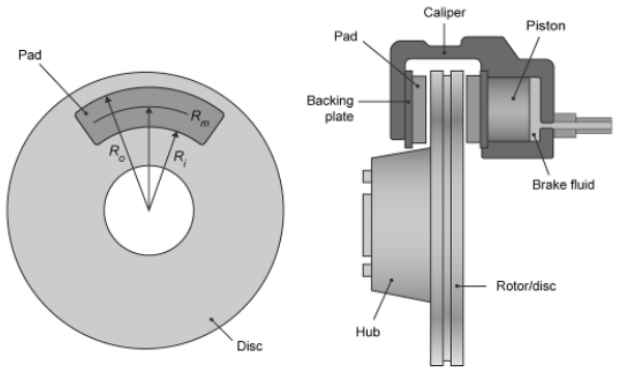

Fig. 19. Brake model.

The numerical values of the parameters employed for modeling the brake system are reported in Table VI.

TABLE VI
BRAKE DATA.

Brake Properties	Data	Units
Nominal radius	0.1	m
Diameter of the brake actuator	0.02	m
Number of pads	2	–
Static friction coefficient	0.9	–
Dynamic friction coefficient	0.7	–
Maximum closing pressure	1.0E+07	Pa

H. Mechanical Differential Model

In this subsection, the model of the mechanical differential is described. The differential is a mechanical organ that distributes the torque between the two drive wheels of the same axle. When cornering, the outer wheel has to follow a trajectory longer than that of the inner wheel. In the absence of a differential, one of the wheels would slip with respect to the plane of rotation, causing considerable wear on the tread, and a lower ability to deal with curves. The mechanical differential is formed by a driving device, the pinion gear which receives the motion from the engine shaft, engaging the ring gear connected with the differential box in which the spider gears are collocated. The end wheels, called planetary wheels, transmit the motion to the respective half-shafts of the driving wheels of the vehicle. The satellite wheels engage with the end wheels and rotate around an axis that is integrated in the differential box. For the planetary gears, the Willis formula is used:

$$\varepsilon = \frac{\omega_a - \Omega}{\omega_b - \Omega} \tag{40}$$

where ε is the gear ratio, ω_a and ω_b are the angular velocity of the left and right planetary wheels, while Ω is the angular velocity of the differential box. This equation yields:

$$\begin{cases} \omega_a = \varepsilon \omega_b + (1-\varepsilon)\,\Omega \\ \omega_b = \frac{1}{\varepsilon}\omega_a - \frac{1-\varepsilon}{\varepsilon}\Omega \\ \Omega = \frac{1}{1-\varepsilon}\omega_a - \frac{\varepsilon}{1-\varepsilon}\omega_b \end{cases} \tag{41}$$

In particular:

$$\varepsilon = -1 \quad \Rightarrow \quad \omega_a + \omega_b = 2\Omega \tag{42}$$

and

$$\begin{cases} \omega_a = -\omega_b + 2\Omega \\ \omega_b = -\omega_a + 2\Omega \\ \Omega = \frac{1}{2}\omega_a + \frac{1}{2}\omega_b \end{cases} \tag{43}$$

Additionally, in the ideal case with unitary mechanical efficiency and transmission ratio, the power balancing equation leads to:

$$T_p \Omega = T_a \omega_a + T_b \omega_b \tag{44}$$

where T_a is the torque associated with the left wheel, T_b is the torque associated with the right wheel, and T_p is the torque associated with the housing of the differential mechanism. Moreover, for the angular momentum balance of the system constituted by the main wheels and the housing, the following relationship must be satisfied:

$$T_p = T_a + T_b \tag{45}$$

Therefore, from Equations (44), (45), and with the use of Equation (41), one obtains:

$$\begin{cases} T_a = \frac{\Omega - \omega_b}{\omega_a - \omega_b} T_p \\ T_b = \frac{\omega_a - \Omega}{\omega_a - \omega_b} T_p \\ \frac{T_a}{T_b} = -\frac{\omega_b - \Omega}{\omega_a - \Omega} \end{cases} \quad \Rightarrow \quad \begin{cases} T_a = \frac{1}{1-\varepsilon} T_p \\ T_b = \frac{\varepsilon}{\varepsilon - 1} T_p \\ \frac{T_a}{T_b} = -\frac{1}{\varepsilon} \end{cases} \tag{46}$$

For a mechanical differential, one has the ideal gear ratio $\varepsilon = -1$. This assumption yields:

$$T_a = T_b = \frac{T_p}{2} \tag{47}$$

Thus, the ideal differential subdivides the driving torque on the two driven shafts in equal parts. In the case of non-unitary mechanical efficiency, and therefore in the presence of losses due to friction inside the mechanism, the power loss P_{loss} is added to the balancing equation:

$$T_p\Omega = T_a\omega_a + T_b\omega_b + P_{loss} \tag{48}$$

which leads to:

$$\begin{cases} T_a = \frac{T_p}{2} - T_{loss} \\ \\ T_b = \frac{T_p}{2} + T_{loss} \end{cases} \tag{49}$$

where T_{loss} is the torque loss. The last equation is precisely the model used to represent the Simulink block chosen. In particular, the parameters used for the differential mechanism are reported in Table VII.

TABLE VII
DIFFERENTIAL MECHANISM DATA.

Differential Properties	Data	Units
Carrier to driveshaft teeth ratio	2	–
Sun-Sun ordinary efficient	85	%
Carrier-driveshaft ordinary efficiencies	92	%
Carrier inertia	0.01	kg×m^2
Planet gear inertia	0.1	kg×m^2

In the case of configuration with two motors, one for each drive wheel, there is no need for a mechanical differential, but it is necessary to simulate its behavior through a so-called electronic differential. Thus, the property of the ideal mechanical differential demonstrated above given by Equation (47) is exploited in the alternative case in which the use of the electronic differential is required.

I. Clutch and Gearbox Models

In this subsection, the models of the clutch and of the gearbox are described. For simplicity, a gearbox with two clutches is used, each coupled to a gearbox, so it is possible to select the gear by choosing which clutch to apply the closing force to. The clutch lock is realized by two flat friction plates that come into contact to transmit the motion. The clutch engages when the pressure of one plate on the other exceeds the engagement threshold. Bidirectional friction is used in order to function both in the positive and negative direction. The block considers the slip angular velocity ω_s equal to the difference between the speed of the driving wheel and that of the driven wheel as described by the following simple equation:

$$\omega_s = \omega_A - \omega_B \tag{50}$$

where ω_A is the angular velocity of the driving wheel and ω_B is the angular velocity of the driven wheel. The dynamic friction torque τ_k is the positive sum between the viscous resistance and the clutch contact torque given by:

$$\tau_k = \tau_v + \tau_c \tag{51}$$

in which:

$$\tau_v = \mu\omega_s, \quad \tau_c = \lambda_k D N R_e P_f A \tag{52}$$

where τ_v is the viscous torque, μ is the viscous coefficient of resistance, τ_c is the torque induced by the contact, λ_k is the kinetic friction coefficient, D is the clutch de-rating factor, N is the number of friction surfaces, A is the engagement surface area, P_f is the threshold clutch pressure, and R_e is the effective torque radius. The clutch de-rating factor D accounts for clutch wear. For a new clutch, D is equal to one. For a clutch approaching the condition of uniform wear, one can write:

$$D = \frac{3}{4}\frac{(r_0 + r_i)^2}{{r_0}^2 + r_0 r_i + {r_i}^2} \tag{53}$$

where r_0 and r_i respectively represent the outer and inner radii of the friction surface modeled as an annular disk. The parameters used for the clutch and gearbox models are reported in Table VIII.

TABLE VIII
CLUTCH AND GEARBOX DATA.

Transmission Properties	Data	Units
Effective torque radius	0.1	m
Number of friction surfaces	4	–
Engagement surface area	0.001	m^2
Kinetic friction coefficient	0.3	–
Clutch de-rating factor	1	–
Threshold clutch pressure	100	Pa
Transmission ratio, configuration 1	9	–
Transmission ratio, configuration 3	9	–
Transmission ratio 1, configuration 2	9	–
Transmission ratio 2, configuration 2	6	–

These data complete the description of the virtual prototype of the electric vehicle realized following a simple model-based system engineering approach.

IV. NUMERICAL RESULTS AND DISCUSSION

In this section, the numerical results found in this investigation are described and a discussion on the performance of the three different design configurations for the electric vehicle devised in this work is provided.

A. Dynamical Simulations

In this subsection, the numerical results obtained from the dynamical simulations performed on the virtual model of the designed electric vehicle are reported. As expected, the behavior of the vehicle model changes for the different configurations analyzed. For example, it is possible to observe the trend of the voltage denoted with V shown in Figure 20. This trend is very similar for the configurations 1 and 2, while in configuration 3 it is slightly larger.

The temperature T reached by the motor can be observed in Figure 21, from which it can be seen that in configuration 3 it is more stable and can be considered approximately constant.

From Figure 22, one can see the difference between the electric power P entering the motor and the actual mechanical power produced. The larger is the difference between the two, the greater are the engine losses.

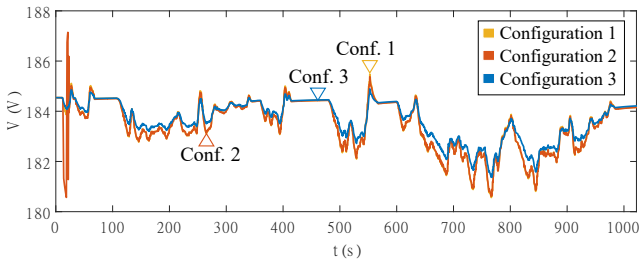

Fig. 20. Comparison of voltages: in yellow the configuration 1, in red the configuration 2, and in blue the configuration 3.

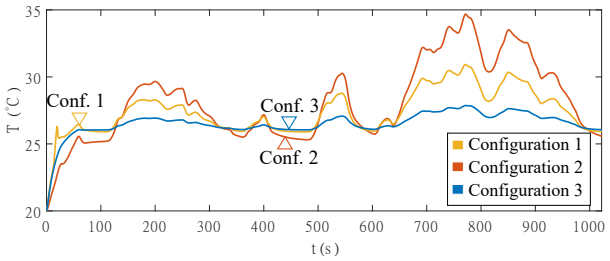

Fig. 21. Comparison of temperatures: in yellow the configuration 1, in red the configuration 2, and in blue the configuration 3.

Figure 23 shows the slip coefficient κ during a cycle for the different configurations, while in Figure 24 the slip velocity denoted with $v_{s,x}$ is represented.

Figures 20, 21, 22, 23, and 24 refer to the three design configurations considered in this work. In particular, in Figures 20, 21, 23, and 24, the yellow curves correspond to configuration 1, the red curves correspond to configuration 2, and the blue curves correspond to configuration 3.

B. Comparative Analysis

In this subsection, the numerical results necessary for performing a quantitative comparative analysis between the three design configurations considered in this investigation focused on the design of an electric vehicle of category L7 are proposed and discussed. In order to perform a comparative study, performance indexes were used to quantitatively compare the three design configurations chosen. As far as the electric performance is concerned, the total electric energy E_{tot} used in a cycle and the energy recovered by regenerative braking E_{rec} are measured and are obtained by using the following equations:

$$E_{tot} = \int_0^T P dt \tag{54}$$

and

$$E_{rec} = \int_0^T P^* dt, \qquad \begin{cases} P^* = 0, & P > 0 \\ P^* = P, & P \leq 0 \end{cases} \tag{55}$$

where t represents the time variable and T denotes the time interval of interest. The average squared deviations for the three degrees of freedom of the vehicle are respectively denoted with E_x, E_z, and E_θ. These parameters are calculated and used as performance indicators for evaluating the quality of the vehicle dynamics. For this purpose, to calculate the errors e_x, e_z, and e_θ, which are respectively associated with

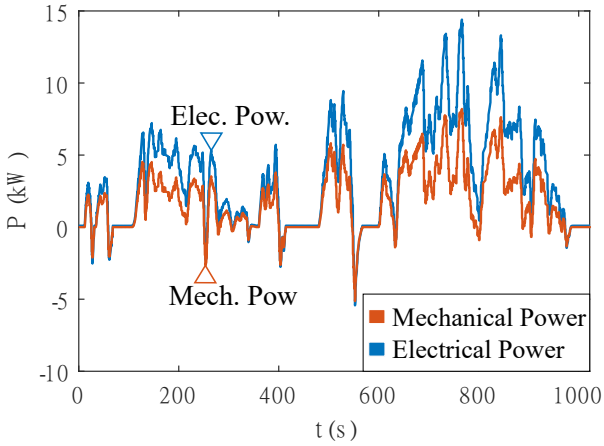

(a) Configuration 1.

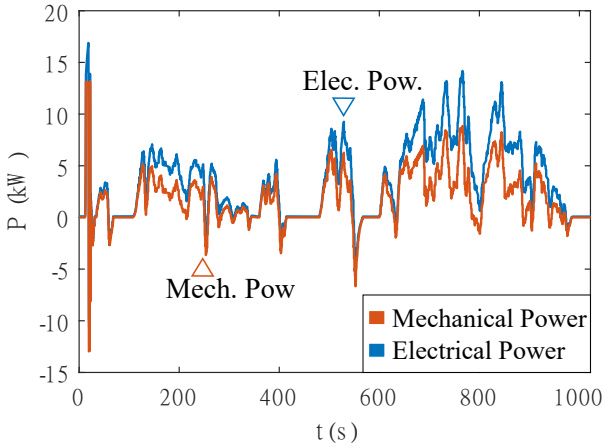

(b) Configuration 2.

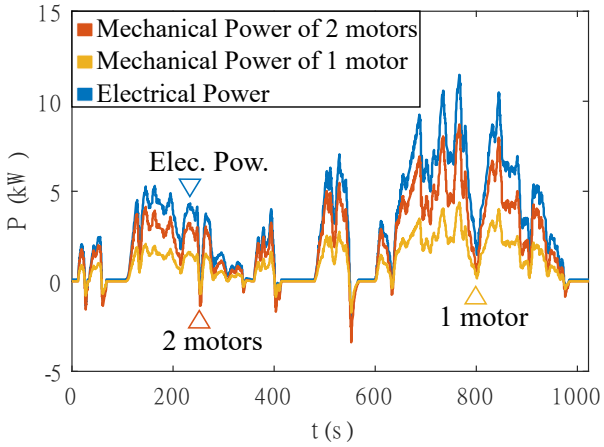

(c) Configuration 3.

Fig. 22. Comparison between electrical and mechanical powers: (a) blue line for electric power, red line for mechanical power of a single motor; (b) blue line for electric power, red line for mechanical power of a single motor; (c) blue line for electric power, yellow line for mechanical power of a single motor, and red line for mechanical power of the two motors.

the degrees of freedom x, z, and θ, the following parameters were used as references:

$$\begin{cases} x_{rif} = x_{WLTP} \\ z_{rif} = -0.4169 \\ \theta_{rif} = -0.015 \end{cases} \tag{56}$$

where the numerical values of z_{rif} and θ_{rif} identify the vehicle equilibrium configuration. By doing so, one can

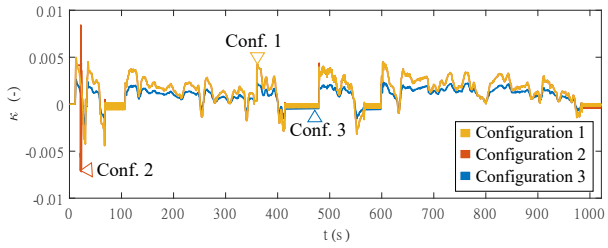

Fig. 23. Comparison of slip coefficients: in yellow the configuration 1, in red the configuration 2, and in blue the configuration 3.

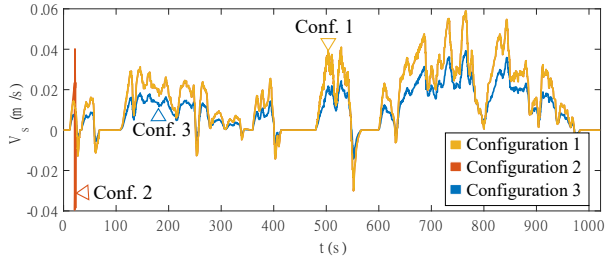

Fig. 24. Comparison of slip velocities: in yellow the configuration 1, in red the configuration 2, and in blue the configuration 3.

write:

$$\begin{cases} e_x = x - x_{rif} \\ e_z = z - z_{rif} \\ e_\theta = \theta - \theta_{rif} \end{cases} \tag{57}$$

Thus, the mean quadratic deviations are given by:

$$\begin{cases} E_x = \frac{1}{T}\int_0^T e_x^2 dt \\ E_z = \frac{1}{T}\int_0^T e_z^2 dt \\ E_\theta = \frac{1}{T}\int_0^T e_\theta^2 dt \end{cases} \tag{58}$$

For understanding the meaning of these numerical values, it is important to specify that the total longitudinal displacement of the vehicle along the x-axis is approximately equal to 8091 m, therefore of the order of kilometers, while the displacement along the normal axis is in the order of millimeters. For this reason, the numerical values obtained along the x-axis are much higher than those computed along the z-axis. Figure 25 shows the trend and the error for the three different degrees of freedom of the electric vehicle.

From the energetic point of view, the numerical results illustrated in Figure 26 and reported in Table IX show that the best configuration is the solution with two electric motors. In fact, compared to the other two, this configuration uses a smaller amount of energy.

TABLE IX
PERFORMANCE PARAMETERS.

Parameter	Conf. 1	Conf. 2	Conf. 3	Units
E_{tot}	0.989	1.002	0.839	kWh
E_{rec}	0.0273	0.0373	0.01025	kWh
$E_{rec,\%}$	2.76	3.72	1.22	%
E_z	3.46E-08	3.45E-08	4.33E-08	m^2
E_θ	5.04E-07	5.07E-08	4.76E-07	rad^2
E_x	2.41	1.18	2.48	m^2

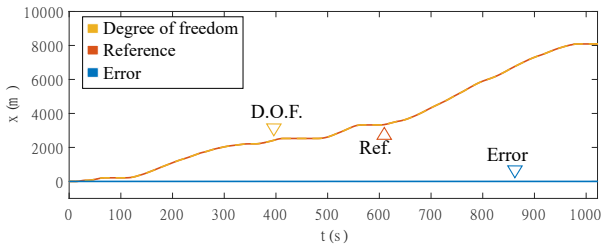

(a) Advancement.

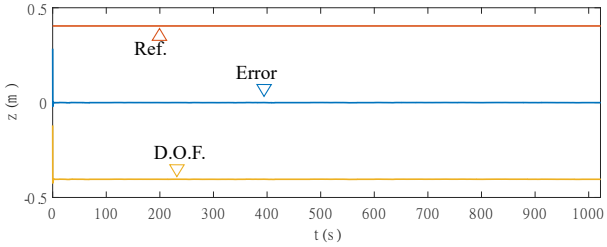

(b) Bouncing.

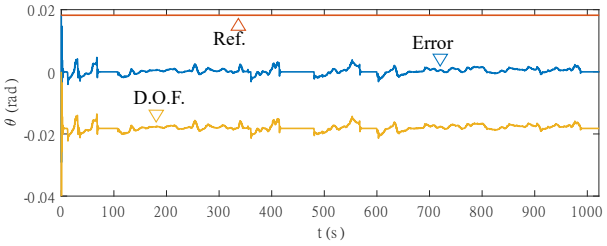

(c) Pitch.

Fig. 25. Comparison of generalized coordinates: in blue lines the errors, in yellow lines the degrees of freedom, and in orange lines the references used.

Nevertheless, the one-engine configuration is a very good choice as well since it uses only 12% more energy when compared with the design solution based on the use of two electric motors. Furthermore, the one-engine configuration is, among the three models, the one that recovers the greater percentage of energy through regenerative braking. The configuration with the gearbox is the most unfavorable, because it uses too much energy, almost twice as much as a two-engine configuration. Considering also the importance of the economic aspects, however, an equally advantageous choice is represented by a model with a single engine and without speed change, because it costs less than one with two engines and, as already indicated, has a relatively low consumption. From the point of view of vehicle dynamics, on the other hand, it can be observed in Table IX that, in the case of the configuration with the speed change, a lower average deviation of the pitch is obtained with respect to the other cases, resulting in the most stable configuration. Moreover, the values of the deviations along the degree of freedom z are quite similar for all configurations. Also, the deviation on the longitudinal distance in the case of the configuration with the gearbox is more than half compared to the other two configurations. This value indicates that this configuration responds better to the closed-loop control system. The final conclusion is, therefore, that the most suitable configuration, from the fundamental energy point of view for a light category L7 vehicle, is the solution with two separate electric engines. The reduced inertia of the

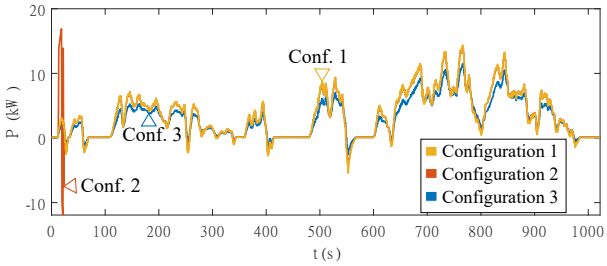

(a) Power.

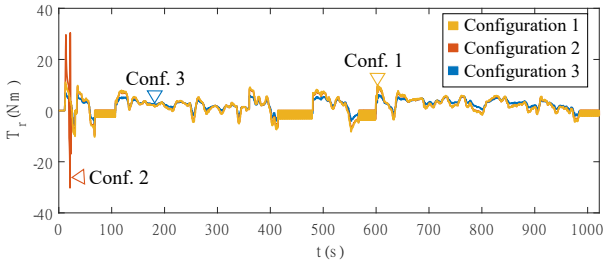

(b) Torque.

Fig. 26. Comparison of power and torque provided in a driving cycle: in yellow the configuration 1, in red the configuration 2, and in blue the configuration 3.

engine, the lightness of the structure, and the absence of mechanical losses due to the transmission components, such as gearbox and mechanical differential, make this design solution more suitable for light vehicles used mainly in urban cycles. This design solution will be used for the actual realization of the physical prototype that will be performed in future investigations.

V. Summary, Conclusions, and Future Work

The authors focus their research mainly on the dynamics of multibody systems [81]–[85], on the optimal control techniques [86]–[90], and on the algorithms of system identification [91]–[95]. Multibody system dynamics deals with the analytical methods and the computational algorithms suitable for carrying out forward and inverse dynamics analysis of mechanical systems whose rigid-flexible components are constrained by mechanical joints. The theory of optimal control is aimed at deriving effective analytical approaches and numerical techniques for obtaining optimal control policies for linear or nonlinear dynamical systems of diverse nature such as multibody mechanical systems. Applied system identification is an emerging scientific discipline that represents the bridge that connects the mathematical domain in which abstract models of dynamical systems are devised with the physical domain in which experimental testing is conducted in order to observe the dynamic behavior of the particular mechanical system of interest. Based on this research background, this paper deals with the design and the development of a virtual prototype of an electric vehicle of class L7 by means of a model-based system engineering approach.

This work is focused on the design of a mathematical model describing the particular aspects that are engineering relevant to an electric vehicle of class L7. The main goal is to be able to carry out an analysis that takes into account the different forces acting on this mechanical system, as well as the different energetic processes that concern the electric vehicle. For this purpose, a standard dynamic model with three degrees of freedom referred to as the half-car model is implemented. In order to simulate appropriate driving cycles, the proposed mechanical model is further extended including also the longitudinal displacement of the vehicle chassis and the vertical displacements of the vehicle wheels. This is also done for considering the stiffness and damping effects induced by the tires, that are schematized employing the Magic Formula of Pacejka typically employed in engineering applications for describing tire models. Once that an adequate computational model is created for the electric vehicle, the computer simulations are performed in the Matlab-Simulink environment. To this end, the Simscape library is employed. Furthermore, the electric propulsion system of the vehicle is also modeled in the Matlab-Simulink environment in order to determine the total energy consumption. In particular, three different configurations are developed for the electric vehicle of interest. This is done in order to make a systematic comparison of the vehicle performance in the three design configurations chosen and, for this purpose, a proportional-integrative controller is employed for regulating the system motion. The control system imposes to the vehicle to follow the standard WLTP (Worldwide harmonized Light vehicles Test Procedure) class 1 driving cycle. The comparison between the design configurations showed that the configuration most advantageous from the energy point of view for a vehicle of category L7 is the design solution composed of two independent engines, each one for each driving wheel, which involve a fixed transmission ratio. On the other hand, if the cost of the configurations is also taken into account, the design solution with a single engine is remarkably advantageous. The final conclusions drawn in this investigation are supported by simulation results obtained by performing numerical experiments on the complete electromechanical vehicle model that serve as a virtual prototype.

Possible future developments could include a more detailed development of the mathematical models describing the physical elements of interest in order to obtain numerical results more in line with an actual laboratory prototype to be constructed. In particular, the control system that manages the speed change and the regenerative braking algorithm could be improved by using more advanced control methods. For example, a proportional-integrative-derivative controller based on an optimal choice of the control constants could be developed by using an adjoint-based nonlinear optimization. Also, an interesting direction of future research related to the study of the nonlinear vehicle dynamics could be the transition from the so-called half-vehicle model to the more detailed full-vehicle model, and this development could be carried out through the multibody modeling approach. Furthermore, by developing a physical prototype, a comparison could be made between the experimental data and those obtained by the computer model that serves as a virtual prototype, so as to be able to verify its reliability and validity. Another interesting idea is to apply the models developed within the recent investigations on control systems for power electronics to other types of motors, allowing the comparison between different electric engines. The important issues mentioned herein will be addressed in future investigations.

AUTHOR CONTRIBUTIONS

This research paper was principally developed by the first author (Carmine Maria Pappalardo). A great support was provided by the second author (Nicola Lombardi). The detailed review carried out by the third author (Domenico Guida) considerably improved the quality of the work.

CONFLICTS OF INTEREST

The authors declare no conflicts of interest.

REFERENCES

[1] B. P. Douglass, *Agile Systems Engineering*, Morgan Kaufmann, 2015.

[2] M. Blundell, and D. Harty, *Multibody Systems Approach to Vehicle Dynamics*, Elsevier, 2004.

[3] R. Turner, "Toward Agile systems engineering processes", *The Journal of Defense Software Engineering*, pp. 11-15, 2007.

[4] E. Andrianarison, and J. D. Piques, "SysML for Embedded Automotive Systems: a Practical Approach", In Conference on Embedded Real Time Software and Systems, IEEE, 2010.

[5] M. H. Sadraey, *Aircraft Design: A Systems Engineering Approach*, John Wiley and Sons, 2012.

[6] F. Villecco, "On the Evaluation of Errors in the Virtual Design of Mechanical Systems", *Machines*, vol. 6, 36, 2018.

[7] P. Sena, P. Attianese, M. Pappalardo, and F. Villecco, "FIDELITY: Fuzzy Inferential Diagnostic Engine for on-LIne supporT to phYsicians", Proceedings of the 4th International Conference on the Development of Biomedical Engineering, Ho Chi Minh City, Vietnam, 8-10 January 2012, IFMBE Proceedings, Springer Verlag: Berlin, Germany, pp. 396-400, 2013.

[8] M. Ghomshei, F. Villecco, S. Porkhial, and M. Pappalardo, "Complexity in Energy Policy: A Fuzzy Logic Methodology", Proceedings of the 6th International Conference on Fuzzy Systems and Knowledge Discovery, Tianjin, China, 14-16 August 2009, IEEE, Los Alamitos, CA, USA, vol. 7, pp. 128-131, 2009.

[9] Y. Zhai, L. Liu, W. Lu, Y. Li, S. Yang, and F. Villecco, "The Application of Disturbance Observer to Propulsion Control of Sub-mini Underwater Robot", Proceedings of the ICCSA 2010 International Conference on Computational Science and Its Applications, Fukuoka, Japan, 23-26 March 2010, Lecture Notes in Computer Science, Springer: Berlin, Germany, pp. 590-598, 2010.

[10] P. Sena, M. D'Amore, M. Pappalardo, A. Pellegrino, A. Fiorentino, and F. Villecco, "Studying the Influence of Cognitive Load on Driver's Performances by a Fuzzy Analysis of Lane Keeping in a Drive Simulation", IFAC Proc. 2013, vol. 46, pp. 151-156, 2013.

[11] M. Ghomshei, and F. Villecco, "Energy Metrics and Sustainability", Proceedings of the International Conference on Computational Science and Its Applications, Seoul, Korea, 29 June - 2 July 2009, Lecture Notes in Computer Science, Springer Verlag, Berlin, Germany, pp. 693-698, 2009.

[12] P. Sena, P. Attianese, F. Carbone, A. Pellegrino, A. Pinto, and F. Villecco, "A Fuzzy Model to Interpret Data of Drive Performances from Patients with Sleep Deprivation", *Comput. Math. Methods Med.*, 868410, 2012.

[13] Y. Zhang, Z. Li, J. Gao, J. Hong, F. Villecco, and Y. Li, "A method for designing assembly tolerance networks of mechanical assemblies", *Math. Probl. Eng.*, 513958, 2012.

[14] F. Villecco, and A. Pellegrino, "Evaluation of Uncertainties in the Design Process of Complex Mechanical Systems", *Entropy*, vol. 19, 475, 2017.

[15] A. Formato, D. Ianniello, F. Villecco, T. L. L. Lenza, and D. Guida, "Design Optimization of the Plough Working Surface by Computerized Mathematical Model", *Emir. J. Food Agric.*, vol. 29, pp. 36-44, 2017.

[16] A. Pellegrino, and F. Villecco, "Design Optimization of a Natural Gas Substation with Intensification of the Energy Cycle", *Math. Probl. Eng.*, 294102, 2010.

[17] A. Formato, D. Guida, D. Ianniello, F. Villecco, T. L. L. Lenza, and A. Pellegrino, "Design of Delivery Valve for Hydraulic Pumps", *Machines*, vol. 6, 44, 2018.

[18] M. A. Jami'in and E. Julianto, "Hierarchical Algorithms of Quasi-Linear ARX Neural Networks for Identification of Nonlinear Systems", *Engineering Letters*, vol. 25, no. 3, pp. 321-328, 2017.

[19] J. Zhang, L. Yu, and L. Ding, "Velocity Feedback Control of Swing Phase for 2-DoF Robotic Leg Driven by Electro-hydraulic Servo System", *Engineering Letters*, vol. 24, no. 4, pp. 378-383, 2016.

[20] Q. W. Guo, W. D. Song, M. Gao, and D. Fang, "Advanced Guidance Law Design for Trajectory-Corrected Rockets with Canards under Single Channel Control", *Engineering Letters*, vol. 24, no. 4, pp. 469-477, 2016.

[21] H. Liu and Y. Li, "Safety Evaluation of a Long-Span Steel Trestle with an Extended Service Term Age in a Coastal Port Based on Identification of Modal Parameters", *Engineering Letters*, vol. 24, no. 1, pp. 84-92, 2016.

[22] I. I. Lazaro, A. Alvarez, and J. Anzurez, "The Identification Problem Applied to Periodic Systems Using Hartley Series", *Engineering Letters*, vol. 21, no. 1, pp. 36-43, 2013.

[23] C. Ratti, and M. Claudel, *The city of tomorrow: Sensors, networks, hackers, and the future of urban life*, Yale University Press, 2016.

[24] D. Offenhuber, and C. Ratti, *Decoding the City: How Big Data Can Change Urbanism*, Birkhauser Verlag GmbH, 2014.

[25] G. Sequenzia, G. Fatuzzo, S. M. Oliveri, and R. Barbagallo, "Interactive re-design of a novel variable geometry bicycle saddle to prevent neurological pathologies", *Int. J. Int. Des. Man.*, vol. 10, pp. 165-172, 2016.

[26] R. Barbagallo, G. Sequenzia, A. Cammarata, S. M. Oliveri, and G. Fatuzzo, "Redesign and multibody simulation of a motorcycle rear suspension with eccentric mechanism", *Int. J. Int. Des. Man.*, vol. 12, pp. 517-524, 2018.

[27] R. Barbagallo, G. Sequenzia, S. M. Oliveri, and A. Cammarata, "Dynamics of a high-performance motorcycle by an advanced multibody/control co-simulation", *P. I. Mech. Eng. K-J-Eng.*, vol. 230, pp. 207-221, 2016.

[28] A. Cammarata, G. Sequenzia, S. M. Oliveri, and G. Fatuzzo, "Modified chain algorithm to study planar compliant mechanisms", *Int. J. Int. Des. Man.*, vol. 10, pp. 191-201, 2016.

[29] S. M. Oliveri, G. Sequenzia, and M. Calí, "Flexible multibody model of desmodromic timing system", *Mech. based Des. Struct.*, vol. 37, pp. 15-30, 2009.

[30] R. Barbagallo, G. Sequenzia, A. Cammarata, and S. M. Oliveri, "An integrated approach to design an innovative motorcycle rear suspension with eccentric mechanism", Advances on Mechanics, Design Engineering and Manufacturing, Springer, Cham, pp. 609-619, 2017.

[31] M. Calí, S. M. Oliveri, and G. Sequenzia, "Geometric modeling and modal stress formulation for flexible multi-body dynamic analysis of crankshaft", 25th Conference and Exposition on Structural Dynamics 2007, IMAC-XXV, pp. 1-9, 2007.

[32] T. K. Tanev, A. Cammarata, D. Marano, and R. Sinatra, "Elastostatic model of a new hybrid minimally-invasive-surgery robot", The 14th IFToMM World Congress, Taipei, Taiwan, October, 2015.

[33] A. Cammarata, "A novel method to determine position and orientation errors in clearance-affected overconstrained mechanisms", *Mechanism and Machine Theory*, vol. 118, pp. 247-264, 2017.

[34] A. Cammarata, I. Calió, A. Greco, M. Lacagnina, and G. Fichera, "Dynamic stiffness model of spherical parallel robots", *Journal of Sound and Vibration*, vol. 384, pp. 312-324, 2016.

[35] M. Callegari, A. Cammarata, A. Gabrielli, and R. Sinatra, "Kinematics and dynamics of a 3-CRU spherical parallel robot", ASME 2007 International Design Engineering Technical Conferences and Computers and Information in Engineering Conference, American Society of Mechanical Engineers, pp. 933-941, 2007.

[36] A. Cammarata, M. Lacagnina, and G. Sequenzia, "Alternative elliptic integral solution to the beam deflection equations for the design of compliant mechanisms", *International Journal on Interactive Design and Manufacturing (IJIDeM)*, pp. 1-7, 2018.

[37] A. Cammarata, R. Sinatra, and P. D. Maddio, "A Two-Step Algorithm for the Dynamic Reduction of Flexible Mechanisms", IFToMM Symposium on Mechanism Design for Robotics, Springer, Cham., pp. 25-32, 2018.

[38] M. Muscat, A. Cammarata, P. D. Maddio, and R. Sinatra, "Design and development of a towfish to monitor marine pollution", *Euro-Mediterranean Journal for Environmental Integration*, vol. 3, 11, 2018.

[39] C. M. Pappalardo, and D. Guida, "On the Computational Methods for Solving the Differential-Algebraic Equations of Motion of Multibody Systems", *Machines*, vol. 6, 20, 2018.

[40] A. Cammarata, and R. Sinatra, "On the elastostatics of spherical parallel machines with curved links", Recent Advances in Mechanism Design for Robotics, Springer, Cham, pp. 347-356, 2015.

[41] A. Cammarata, M. Lacagnina, and R. Sinatra, "Dynamic simulations of an airplane-shaped underwater towed vehicle marine", Computational Methods in Marine Engineering V - Proceedings of the 5th International Conference on Computational Methods in Marine Engineering, 2013.

[42] A. Cammarata, M. Lacagnina, and R. Sinatra, "Closed-form solutions for the inverse kinematics of the Agile Eye with constraint errors on the revolute joint axes", IEEE/RSJ International Conference on Intelligent Robots and Systems (IROS), pp. 317-322, 2016.

[43] A. Cammarata, J. Angeles, and R. Sinatra, "Kinetostatic and inertial conditioning of the McGill Schonflies-motion generator", *Advances in Mechanical Engineering*, vol. 2, 186203, 2010.

[44] A. Cammarata, "Unified formulation for the stiffness analysis of spatial mechanisms", *Mechanism and Machine Theory*, vol. 105, pp. 272-284, 2016.

[45] A. Cammarata, "Optimized design of a large-workspace 2-DOF parallel robot for solar tracking systems", *Mechanism and machine theory*, vol. 83, pp. 175-186, 2015.

[46] Y. G. Liao, and H. I. Du, "Cosimulation of Multi-Body-Based Vehicle Dynamics and an Electric Power Steering Control System", *Proceedings of the Institution of Mechanical Engineers, Part K: Journal of Multi-body Dynamics*, 215, pp. 141-151, 2001.

[47] J. Urruzola, A. Suescun, J. T. Celigueta, J. Pargada, M. Perez, and S. Ausejo, "Integration of Multibody Systems in Mechatronic Simulation Environments of Any Kind", *International journal of vehicle design*, 28, pp. 57-67, 2002.

[48] G. J. Choi, Y. M. Yoo, K. P. Lees, and Y. S. Yoon, "A Real-Time Multibody Vehicle Dynamic Analysis Method using Suspension Composite Joints", *International Journal of Vehicle Design*, 24, pp. 259-273, 2000.

[49] J. Y. Yong, V. K. Ramachandaramurthy, K. M. Tan, and N. Mithulananthan, " A review on the state-of-the-art technologies of electric vehicle, its impacts and prospects", *Renewable and Sustainable Energy Reviews*, 49, pp. 365-385, 2015.

[50] M. Santucci, M. Pieve, and M. Pierini, "Electric L-category vehicles for smart urban mobility", *Transportation Research Procedia*, 14, pp. 3651-3660, 2016.

[51] M. Guiggiani, *The science of vehicle dynamics*, Springer Netherlands, 2014.

[52] J. T. Cao, H. H. Liu, P. Li, D. J. Brown, and G. Dimirovski, " A study of electric vehicle suspension control system based on an improved half-vehicle model", *International Journal of Automation and Computing*, vol. 4, no. 3, pp. 236-242, 2007.

[53] D. J. Brown, and G. Dimirovski, "A study of electric vehicle suspension control system based on an improved half-vehicle model", *International Journal of Automation & Computing*, 7, pp. 56-61, 2007.

[54] H. B. Pacejka, *Tyre and vehicle dynamics*, Butterworth-Heinemann, ISBN 0, 7506(5141), 2006.

[55] T. Vo-Duy, and M. C. Ta, "A signal hardware-in-the-loop model for electric vehicles", *Robomech Journal*, vol. 3, no. 1, 29, 2016.

[56] C. F. Androne, S. B. Rao, "Vehicle Simulation for Powertrain System Testing", 2017.

[57] V. D. Thanh, D. Q. Thinh, N. B. Huy, and T. C. Minh, " Design of Hardware-in-the-loop Model for Electric Vehicles", Proceeding of Publishing House for Science and Technology, vol. 1, no. 1, 2016.

[58] J. De Santiago, H. Bernhoff, B. Ekergard, S. Eriksson, S. Ferhatovic, R. Waters, and M. Leijon, "Electrical motor drivelines in commercial all-electric vehicles: A review", *IEEE Transactions on vehicular technology*, vol. 61, no. 2, pp. 475-484, 2012.

[59] N. Gawai, D. Yadav, S. Chavan, A. Lele, and S. Dalvi, " Design, modelling & analysis of double wishbone suspension system", *Int. J. Mech. Engg. and Robotics*, vol. 4, no. 1, pp. 58-62, 2016.

[60] M. Azman, P. D. King, and H. Rahnejat, "Combined bounce, pitch, and roll dynamics of vehicles negotiating single speed bump events", . *Proceedings of the Institution of Mechanical Engineers, Part K: Journal of Multi-body Dynamics*, vol. 221, no. 1, pp. 33-40, 2007.

[61] E. Tanik, and V. Parlaktas, "Design of a very light L7e electric vehicle prototype", *International Journal of Automotive Technology*, vol. 16, no. 6, pp. 997-1005, 2015.

[62] M. Leijon, B. Ekergard, S. Apelfrojd, J. De Santiago, H. Bernhoff, R. Waters, and S. Eriksson, "On a Two Pole Motor for Electric Propulsion System", *International Journal of Engineering Science and Innovative Technology*, vol. 2, no. 1, pp. 99-111, 2013.

[63] Y. Yang, K. Arshad-Ali, J. Roeleveld, and A. Emadi, "State-of-the-art electrified powertrains-hybrid, plug-in, and electric vehicles", *International journal of powertrains*, vol. 5, no. 1, pp. 1-29, 2016.

[64] A. Albinsson, and C. Routledge, "The damper levels influence on vehicle roll, pitch, bounce and cornering behaviour of passenger vehicles", 2013.

[65] R. Di Martino, "Modelling and Simulation of the Dynamic Behaviour of the Automobile", Doctoral dissertation, Université de Haute Alsace-Mulhouse, 2005.

[66] A. Nair, and K. R. Rajagopal, "Generic model of an electric vehicle for dynamic simulation and performance prediction", IEEE 2010 International Conference on Electrical Machines and Systems, pp. 753-757, 2010.

[67] C. C. Lin, Z. Filipi, Y. Wang, L. Louca, H. Peng, D. N. Assanis, and J. Stein, "Integrated, feed-forward hybrid electric vehicle simulation in SIMULINK and its use for power management studies", *SAE*, 2001-01-1334, 2001.

[68] T. A. T. Mohd, M. K. Hassan, and W. M. K. A. Aziz, "Mathematical modeling and simulation of an electric vehicle", *Journal of Mechanical Engineering and Sciences*, vol. 8, no. 1, pp. 1312-1321, 2015.

[69] H. Xiaoling, and W. Hodgson Jeffrey, "Modeling and Simulation for Hybrid Electric Vehicles-Part I: Modeling", *IEEE Transactions on Intelligent Transportation Systems*, vol. 3, pp. 244-251, 2002.

[70] W. Lee, D. Choi, and M. Sunwoo, "Modelling and simulation of vehicle electric power system", *Journal of Power Sources*, vol. 109, no. 1, pp. 58-66, 2002.

[71] B. Tabbache, A. Kheloui, and M. E. H. Benbouzid, "An adaptive electric differential for electric vehicles motion stabilization", *IEEE Transactions on Vehicular Technology*, vol. 60, no. 1, pp. 104-110, 2011.

[72] D. W. Gao, C. Mi, and A. Emadi, "Modeling and simulation of electric and hybrid vehicles", *Proceedings of the IEEE*, vol. 95, no. 4, pp. 729-745, 2007.

[73] R. C. Kroeze, and P. T. Krein, "Electrical battery model for use in dynamic electric vehicle simulations", 2008 IEEE Power Electronics Specialists Conference, pp. 1336-1342, 2008.

[74] D. McDonald, "Electric vehicle drive simulation with matlab/simulink", Proceedings of the 2012 North-Central Section Conference, 2012.

[75] M. Ehsani, Y. Gao, S. Longo, and K. Ebrahimi, *Modern electric, hybrid electric, and fuel cell vehicles.*, CRC press, 2018.

[76] C. M. Pappalardo, "A natural absolute coordinate formulation for the kinematic and dynamic analysis of rigid multibody systems", *Nonlinear Dynamics*, vol. 81, no. 4, pp. 1841-1869, 2015.

[77] C. M. Pappalardo, and D. Guida, "A time-domain system identification numerical procedure for obtaining linear dynamical models of multibody mechanical systems", *Archive of Applied Mechanics*, vol. 88, no. 8, pp. 1325-1347, 2018.

[78] M. A. Gonc, W. B. Lenz, M. A. Ribeiro, A. M. Tusset, and J. M. Balthazar, "Magneto rheological damper in semi-active vehicle suspension system using SDRE control for a half car model", *Journal— MESA*, vol. 10, no. 1, pp. 75-91, 2019.

[79] J. Cabrera, J. Castillo, J. Perez, J. Velasco, A. Guerra, and P. Hernandez, "A procedure for determining tire-road friction characteristics using a modification of the magic formula based on experimental results", *Sensors*, vol. 18, no.3, 896, 2018.

[80] R. C. Hibbeler, *Engineering mechanics*, Pearson education, 2001.

[81] M. C. De Simone, Z. Rivera, and D. Guida, "Obstacle avoidance system for unmanned ground vehicles by using ultrasonic sensors", *Machines*, vol. 6, no. 2, 18, 2018.

[82] M. C. De Simone, S. Russo, Z. B. Rivera, and D. Guida, "Multibody model of a UAV in presence of wind fields", Proceedings of the 2017 International Conference on Control, Artificial Intelligence, Robotics & Optimization (ICCAIRO), pp. 83-88, 2017.

[83] M. C. De Simone, and D. Guida, "Identification and Control of a Unmanned Ground Vehicle By using Arduino", *UPB Scientific Bulletin*, vol. 80, pp. 141-154, 2018

[84] M. C. De Simone, and D. Guida, "On the development of a low-cost device for retrofitting tracked vehicles for autonomous navigation", AIMETA 2017 - Proceedings of the 23rd Conference of the Italian Association of Theoretical and Applied Mechanics, vol. 4, pp. 71-82, 2017.

[85] M. C. De Simone, and D. Guida, "Control design for an under-actuated UAV model", *FME Transactions*, vol. 46, pp. 443-452, 2018.

[86] M. C. De Simone, and D. Guida, "Modal coupling in presence of dry friction", *Machines*, vol. 6, no. 1, 8, 2018.

[87] M. C. De Simone, Z. B. Rivera, and D. Guida, "Finite element analysis on squeal-noise in railway applications", *FME Transactions*, vol. 46, pp. 93-100, 2018.

[88] C. M. Pappalardo and D. Guida, "System Identification and Experimental Modal Analysis of a Frame Structure", *Engineering Letters*, vol. 26, no. 1, pp. 56-68, 2018.

[89] A. Concilio, M. C. De Simone, Z. B. Rivera, and D. Guida, "A new semi-active suspension system for racing vehicles", *FME Transactions*, vol. 45, pp. 578-584, 2017.

[90] A. Quatrano, M. C. De Simone, Z. B. Rivera, and D. Guida, "Development and implementation of a control system for a retrofitted CNC machine by using Arduino", *FME Transactions*, vol. 45, pp. 565-571, 2017.

[91] A. Ruggiero, S. Affatato, M. Merola, and M. C. De Simone, "FEM analysis of metal on UHMWPE total hip prosthesis during normal walking cycle", AIMETA 2017 - Proceedings of the 23rd Conference of the Italian Association of Theoretical and Applied Mechanics, vol. 2, pp. 1885-1892, 2017.

[92] A. Ruggiero, M. C. De Simone, D. Russo, and D. Guida, "Sound pressure measurement of orchestral instruments in the concert hall of a public school", *International Journal of Circuits, Systems and Signal Processing*, vol. 10, pp. 75-81, 2016.

[93] M. C. De Simone, and D. Guida, "Dry friction influence on structure dynamics", COMPDYN 2015 - 5th ECCOMAS Thematic Conference on Computational Methods in Structural Dynamics and Earthquake Engineering, Crete Island, Greece, pp. 4483-4491, 2015.

[94] C. M. Pappalardo and D. Guida, "Development of a New Inertial-based Vibration Absorber for the Active Vibration Control of Flexible Structures", *Engineering Letters*, vol. 26, no. 3, pp. 372-385, 2018.

[95] C. M. Pappalardo and D. Guida, "On the dynamics and control of underactuated nonholonomic mechanical systems and applications to mobile robots", *Archive of Applied Mechanics*, vol. 89, no. 4, pp. 669-698, 2019.